CRYSTAL PRESSURE OF PHARMACEUTICALS IN NANOSCALE PORES

by

Emily Anne Berglund

A thesis submitted in partial fulfillment
of the requirements for the degree

of

Master of Science

in

Chemical Engineering

MONTANA STATE UNIVERSITY
Bozeman, Montana

April 2017

ACKNOWLEDGEMENTS

iii

TABLE OF CONTENTS

LIST OF TABLES

Table   Page

LIST OF FIGURES

LIST OF FIGURES — CONTINUED

ABSTRACT

Many pharmaceutical compounds are poorly soluble in water. This is problematic because most pharmaceuticals are delivered orally and must dissolve in the gastrointestinal fluid to be absorbed by the body. Drug dissolution rate is proportional to surface area, so a common formulation strategy is to structure drugs as small as possible to maximize surface area. A simple approach to create very small particles is to structure the compounds within the nanoscale pore space of a colloidal packing. The resulting composite undergoes rapid disintegration in water and the exposed drug exhibits dramatically improved dissolution rates. We hypothesize that composite breakup is driven by the growth of nanoscale crystals, which exert a pressure on the walls of the confining pores. To test this hypothesis, we systematically vary the amount of water permitted into the composite and use calorimetry to monitor the evolution of the crystal size distribution as a function of water content. To exert sufficient pressure to overcome the tensile yield stress of the composite, the crystals must be fed by a supersaturated phase. Our results suggest that differences in crystal curvature due to crystal confinement and crystal size polydispersity generate the necessary supersaturation. These results are relevant not just for drug formulations, but for understanding physical processes such as salt damage to buildings and road damage due to frost heave.

CHAPTER ONE

INTRODUCTION

Nearly half of the US population have taken a prescription drug in the past 30 days.[1] Oral dosage forms are the most convenient pharmaceutical administration method and are thus the most common dosage form.[2] When drugs are taken orally, they enter the gastrointestinal tract, dissolve in the gastrointestinal fluid and are absorbed through the gastrointestinal membrane; thus, two properties, aqueous solubility and intestinal permeability dictate the efficacy of oral dosage forms. The efficacy of drug absorption is quantified as the fraction of active drug that reaches the circulatory system and is made "bioavailable".[3] Intravenous drugs, which are injected straight into the circulatory system, have a bioavailability of one. By contrast, the bioavailability of oral drugs is always less than one as some active drug is always lost as it passes through the gastrointestinal system. Improving the bioavailability of oral dosage forms requires methods of enhancing gastrointestinal solubility and permeability.

Solubility, in this context, refers to the maximum concentration of drug that can dissolve in the gastrointestinal fluid.[3] Interestingly, it is not equilibrium solubility that typically limits bioavailability, but the fact that drugs with poor solubility dissolve very slowly. The dissolution rate of a solid is described by the Noyes-Whitney equation, Equation 1.1.

$$\frac{dM}{dt} = \frac{DA}{h}(C_s - C_x)$$
(Eqn. 1.1)

Because the dissolution rate, in units of mass per unit time, $\frac{dM}{dt}$ is directly proportional to the difference between the drug saturation concentration, C_s, and drug concentration in the bulk solution, C_x, a drug with a low saturation solubility also dissolves very slowly. Here, D is the diffusion coefficient, A is the total surface area of the solid form, and h is the hydrodynamic layer thickness. The dissolution rate can be increased by reducing the hydrodynamic layer thickness through stirring or by increasing the surface area of the drug. A faster dissolution rate allows the systemic system more opportunity to absorb the drug before excretion, depending on permeability, and is the aim of this study.

Permeability is related to the extent of absorption and mass transfer rate across the human intestinal wall, measured as a fraction of solubilized drug reaching the systemic system. A "highly permeable" drug has an absorption rate of at least 90% of the administered dose.[3] These important parameters inspired the development of a drug classification system called the Biopharmaceutics Classification System (BCS), composed of four classes shown in Figure 1.1.[3]
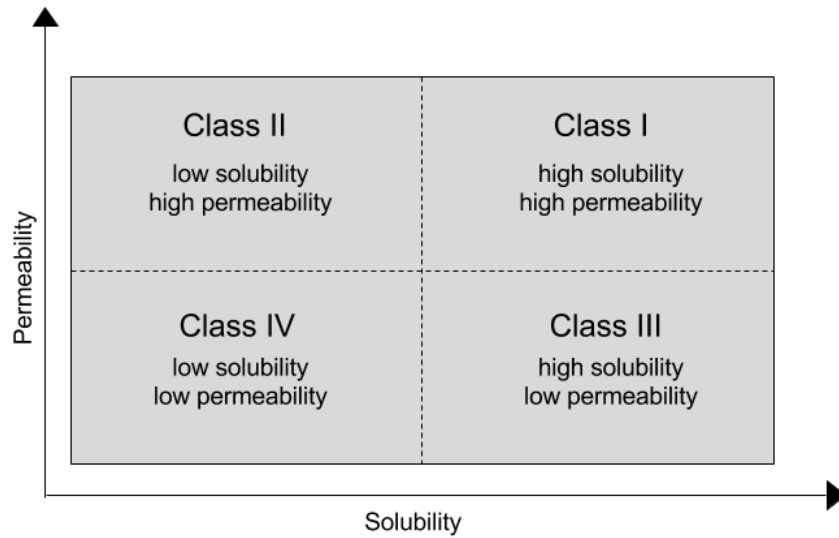
Figure 1.1. The Biopharmaceutics Classification System illustrating the four classes of drugs dictated by relative permeability and solubility properties.[3]

Drugs with high solubility and high permeability (Class I) are ideal for oral delivery, as they achieve the highest bioavailability. These drugs dissolve quickly in the gastrointestinal tract and are absorbed well across the intestinal membrane. By contrast, Class IV drugs do not dissolve well in the stomach and do not cross the gastrointestinal tract effectively. Thus, Class IV drugs have the lowest bioavailability. Drugs that fall into the remaining two classifications are also not ideal for oral delivery, and have one efficacy-limiting property. Class II pharmaceuticals are drugs that have low solubility, but high gastrointestinal permeability. Nearly 1/3 of all drugs fall into this category.[4] Altering permeability properties of pharmaceutical systems prove much more difficult than improving dissolution rates. Due to their popularity and adjustable dissolution rate, as depicted by the Noyes-Whitney equation, Class II drugs were chosen as the focus of this study.

There are currently several formulation techniques to enhance the dissolution rates of low solubility drugs. Different formulation strategies target different properties of drugs that greatly contribute to their low solubility. These physiochemical properties range from hydrophobicity to crystallinity and pH. Lipid formulations are, arguably, the fastest growing interest group of low solubility drug modifications.[5] These non-solid oral formulations consist of dissolving the drug in hydrophilic or lipophilic surfactants, commonly referred to as oral capsules.[5] The goal with this strategy is to suspend the drug in a dissolved state through the gastrointestinal tract.[6] While this technique faces many challenges, one of the largest is finding a surfactant that is safe to ingest for encapsulation. Commonly used surfactants include docusate sodium and Pluronic-F68.[7]

Chemical modifications are also useful for increasing drug solubility, and include strategies such as salt formation.[7] Salt formation is the most useful technique for solubility enhancement of drugs that are very acidic or basic.[8] Salt formation strategies utilize the knowledge that the conjugate bases and conjugate acids of acidic and basic compounds, respectively, have higher solubilities than their counter forms.[8] Thus, to achieve higher solubilities, the conjugate acid or base of a low solubility drug is precipitated with an appropriate counter ion.[8] This precipitated salt form has a higher solubility than its non-salt form. An important consideration with the use of salt formation is the potentially harmful effects of drug structure manipulation.[7]

Physical modifications, specifically particle size reduction, are among the most commonly practiced formulation alteration methods.[6] Techniques such as micronization have proved effective in increasing solubility. Micronization involves grinding or

pulverizing the drug to reduce the size of drug particle.[6] Reducing the particle size increases the surface area to volume ratio, thus increasing the contact area of fluid and drug and subsequently solubility.[9] As previously described, the Noyes-Whitney equation indicates an increase in surface area increases the dissolution rate. Thus, particle reduction can allow Class II drugs to more closely mimic the ideal bioavailability of Class I drugs.

A drug particle reduction method is explored here, implementing a porous media to increase drug surface area. More specifically, this study proposes a tablet production method in which colloidal silica particles are slip cast, and interstitial spaces are imbibed with melted drug. When a subclass of Class II drugs, those with a melting temperature under 120°C, are imbibed into a silica template then placed in water, dramatic composite breakup is observed as shown in Figure 1.2. This dramatic breakup leads to an enhanced dissolution rate, increasing drug bioavailability. The experimental methods associated with this formulation approach are outlined in Chapter 2. Understanding the physical mechanism driving this surprising composite breakup is the focus of the remainder of this thesis.
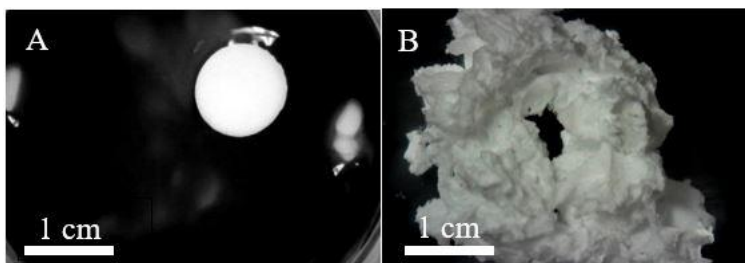

Figure 1.2. Photographs depicting the dramatic break up of a fenofibrate-imbibed colloidal silica template (A) immediately after being placed in water and (B) five minutes after being placed in water.

In this study, we find that the loss of mechanical integrity of our composites can be attributed to crystal pressure. This is a well-studied phenomenon, and is implicated in weather-related damage to road surfaces and monuments.[1] Road surfaces are typically damaged by the growth of ice crystals and monuments are damaged by the growth of salt crystals.[1,10] In both cases, if the pressure exerted by a growing crystal exceeds the yield strength of the confining pore, breakup can occur. The same mechanism, crystal pressure, may be responsible for our low solubility composite breaking. Drug crystals, confined by colloidal silica beads, rearrange and grow, exerting a pressure on the walls of the silica. When this pressure overcomes the yield strength of the silica, breakup occurs.

For crystals to grow, they must be in contact with a supersaturated solution, composed of a solvent and solute. In our system, the solvent is water and solute is drug. So, for a supersaturated solution to exist, water must be able to enter the composite. Chapter 2 details the formulation method and preliminary data. Chapter 3 describes the use of capillary condensation to quantify a network of nanoscale cracks, which allow water to enter the composite. Chapter 4 describes the use of differential scanning calorimetry (DSC) to follow changes in drug crystallinity and the structural evolution of the crystal size distribution as a function of water content in the nanoscale cracks. Appendix A describes the use of hydrogen nuclear magnetic resonance (H-NMR) to follow conformational changes in the confined drug, and to establish a time-scale for initial crystallization due to quenching. Finally, preliminary Raman spectroscopy measurements are discussed in Appendix B.

CHAPTER TWO

FORMULATION METHOD AND PRELIMINARY DATA

A formulation method was developed to manufacture composites of colloidal silica and drug consistently. To begin, a block of plaster (calcium sulfate hemihydrate) was cleaned by scraping the top layer off using a clean razor blade. The block was then rinsed in distilled water and left to dry for 24 hours. After the block of gypsum had dried, sterile 1 mL pipette tips were cut such that they had a desired length of about two centimeters with a constant radius. The cut pipette tips, tablet molds, were then placed atop the plaster blocks, and 300 uL of colloidal silica suspended in water (Nissan Chemical, MP-1040-H, d = 100nm) was pipetted into the molds. This is a common method of eliminating water from a material known as slip casting. The filled molds were left at ambient conditions for 24 hours, then the tablets were removed by gently lifting the molds from the gypsum, depicted below in Figure 2.1. At this point in the process the tablets were a hard, porous material.
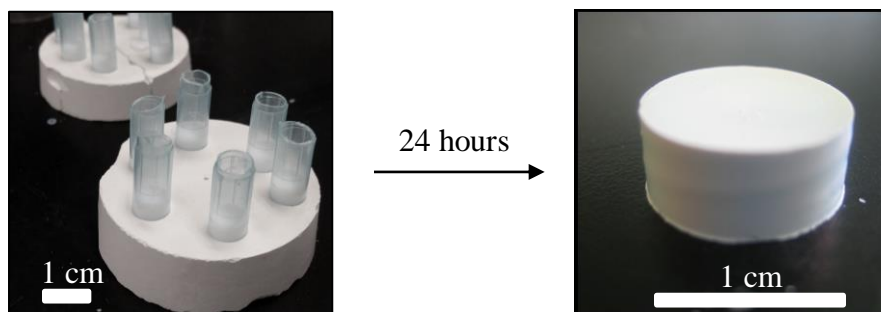

24 hours

Figure 2.1. The colloidal silica slip casting process. Image A depicts 300 uL of colloidal silica contained within molds made from cut 1 mL pipette tips. After 24 hours, the tablet was removed from the molds gently, shown in image B.

After the silica tablets were slip cast, drug was melted at a temperature ten degrees Celsius higher than its melting temperature. A clean glass microscope slide was placed on a hot plate at the desired temperature, here ten degrees Celsius higher than the melting point of fenofibrate, 90°C. Pure, powdered fenofibrate (TCI, F0674) was then heaped on top of the glass slide. Once the drug was melted, a silica tablet was placed on top. After about 30 minutes the color of the composite turned translucent, indicating complete imbibition. This indication was possible due the matching refractive indices of the drug and silica. Once completely imbibed, the composite was removed from the hot plate via tweezers, and was quickly wiped off with a clean tissue. This was done to remove excess drug from the outside of the composite. The composite was then placed in a desiccant chamber (Drierite) for at least 72 hours, then either tested or moved into a chamber with a controlled relative humidity to satisfy a given protocol. Variations of this protocol were made, depending on experimental design, but the imbibition process stayed constant through all experiments.

In Chapter 3, the evolution of microstructure of the composite is analyzed as a function of water condensed inside the pores. To analyze them, they were exposed to varying relative humidities and weighed. More specifically, once the nine tablets were imbibed with fenofibrate, they were placed in a desiccant chamber (0.0 relative humidity, Drierite) for three days. They were then weighed on an analytical balance, and weights were recorded as the initial weight (in milligrams). After this they were distributed into varying relative humidity chambers: 0.0, 0.25, 0.43, 0.75, 0.84, 0.86, 0.90, 0.97, and 1.0. The tablets were weighed on an analytical balance every two hours for 10 hours, then about

every four hours for an additional five data points, and finally every 12 hours for two more data points. This data was then used to quantify the pore size distribution within the composites.

In Chapter 4 smaller composites were made by slip casting a smaller volume of colloidal silica to reduce their size to fit into DSC sample pans. In this method, only 30 uL were pipetted on the gypsum, into cut 200μL pipette tips. Twenty-seven composites were manufactured – three for each humidity. After imbibition, they were kept in a relative humidity of 0.0. They were contained in the glass vessel with Drierite for three days. They were then distributed evenly into nine different relative humidity chambers: 0.0, 0.25, 0.43, 0.75, 0.84, 0.86, 0.90, 0.97, and 1.0. The composites were enclosed in these chambers for three days. This was enough time for the pores to saturate, as demonstrated in the pore analysis chapter. After this, the composites were transferred back to the desiccant chamber for an additional three days. This was done to drive off residual water, as DSC is a method in which the composites are heated and thus are susceptible to data interference from the effects of water boiling. Twenty-seven hermetically sealable DSC pans were then weighed and recorded. The three composites from each relative humidity were then weighed on an analytical balance, and hermetically sealed inside their corresponding pans.

A DSC program was constructed in the TA Instruments program designed for the specifically for the Discovery Series DSC. Each pan was designated a number corresponding with the position they occupied in the autosampler. Every composite was exposed to the same regime: a ramp rate of 1ºC/min, starting at 35ºC and ending at 95ºC.

Once a composite was exposed to this, it was removed from the sampling station and the system cooled back down to 35°C before beginning the next experiment.

The main formulation strategy above was initially developed by Dr. James Wilking and Dr. Andre Studart at Harvard University. Moreover, at Harvard, several experiments were conducted to understand the composition of the silica-fenofibrate system and establish trends in breakup. First, micrographs of an unimbibed and imbibed tablet were taken using a Scanning Electron Microscope (SEM), shown below in Figure 2.2. This was done to gain qualitative insight into the structure of the tablet, and understand the packing of the silica beads. The figure below clearly shows void spaces created by the random close packing of the silica beads before imbibition (left), and the decrease in void pore space after imbibition (right).
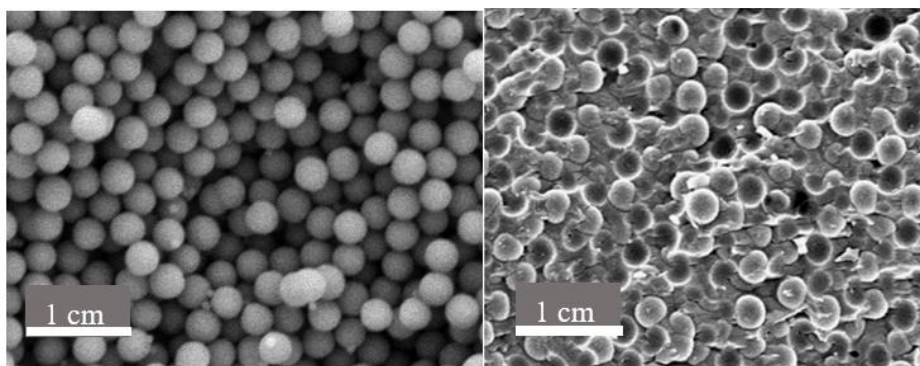
Figure 2.2. The image on the left is a SEM image of an unimbibed tablet, showing the void spaces created by the random close packing of the silica beads. The image on the right is of a silica tablet imbibed with fenofibrate, illustrating less available void pore spaces.

After gaining a qualitative understanding of the composition of the composite, several experiments were conducted to develop breakup constraints. The first was placing an unimbibed tablet in water. A tablet of unimbibed silica was placed in water and no

breakup is observed. This suggested the breakup was due to drug interactions with the system. The silica tablet was then imbibed with different organic drugs and dropped in water. This was tested by Dr. James Wilking at Harvard University, to discern any trend in breakup occurrence. The data from this showed only drugs with a melting temperature equal to or below 120°C break apart. To explore this trend further, a drug that was known to induce breakup, fenofibrate, was heated above 120°C. The melting point of fenofibrate is 80°C, and was usually imbibed at 90°C. This was done to test whether the melting point trend was an artifact of the imbibition process instead of the properties of the drug. If the fenofibrate composite imbibed at 120°C didn't break, it would indicate that breakup was a result of heating and quenching the tablet. The tablet did, in fact, break up. This suggested that the melting point trend observed was due to chemical properties, not the imbibition process.

CHAPTER THREE

PORE ANALYSIS

For a crystal to exert pressure on the confining walls of a pore space, crystal growth must be fed by a supersaturated solution.[11] This requires that interconnected cracks must exist, which allow water to first enter the composite. Fenofibrate shrinks by about five percent in volume when it crystallizes from a liquid to a solid; thus, it is reasonable to assume that this shrinkage results in nanoscale cracks and voids. Several experiments were designed to test this hypothesis both qualitatively and quantitatively.

To gain qualitative insight into the possible existence of nanoscale cracks, a fenofibrate-silica composite was placed in a shallow dish containing water. A front was observed propagating through the composite, exposing cracks in the microstructure, but was difficult to see due to the opaque color of the composites and translucence of water. Thus, a composite was placed in an aqueous dye solution. The aqueous dye solution was only in contact with the bottom of the composite, and thus had to propagate from the bottom to the top, where imaging took place. Time lapse images were obtained every few seconds, capturing the transport of dye through the composite. After about 30 seconds in the dye, no front of dye had reached the top layer of the composite (Fig. 3.1B). After another 50 seconds, dye was starting to reach the top (Fig. 3.1C). This was followed by dye rapidly reaching the top, in a quasi-uniform front (Fig 3.3D, 3.3E, 3.3F). Breakup was seen after the front reached the top of the composite. The time lapse showed a network of cracks within the composite acting as a transport system for water. Images from this time-lapse

experiment are shown in Figure 3.1. This simple experiment suggested water is, in fact, being transported through the composite over time.
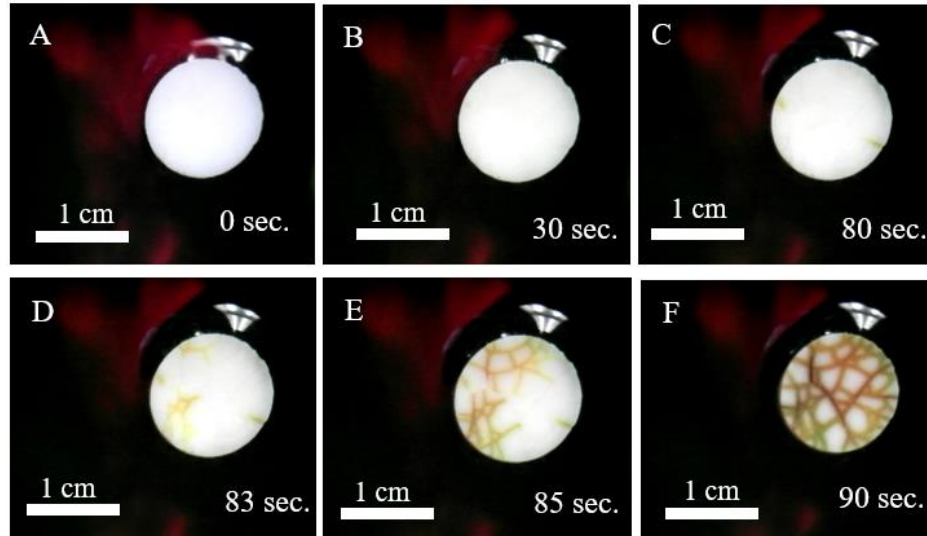

Figure 3.1. A composite partially submerged in food coloring to observe the transport of an aqueous dye solution propagate through a network of cracks (A). After 30 seconds, no front of dye is seen on the top of the composite (B). Fifty seconds later, dye makes its first appearance on the surface (C). A front of dye then quickly reaches the surface of the composite in a matter of seconds, exposing the complex nature of cracks acting as a transport system in the composite (D, E, F).

To quantify the crack network, several composites were subjected to varying relative humidities of 0.0, 0.25, 0.43, 0.75, 0.84, 0.86, 0.90, 0.97, and 1.0 for three days. The composites were then weighed while in their respective humidity chambers. Saturated salt solutions were made to set varying relative humidities in different chambers, via chemical potential (activity) equilibrium.[12] Solutions were made from distilled water and chemically pure salts, creating slurry mixtures. These mixtures were then placed in glass containers and allowed to equilibrate for three days, at ambient temperature. This equilibrium vapor pressure of the saturated salt solution at a set temperature, relative to the

vapor pressure associated with water at those same conditions, is known as the relative humidity.[12] The advantage of using a saturated salt solution, in contrast to a salt solution, is that the relative humidity theoretically remains constant even if water enters or leaves the chamber. In other words, it is a far more stable system. Since each salt is only able to produce one relative humidity at the desired temperature (ambient conditions), eight saturated salt solutions were made ranging from about 0.23 to 0.97. To set the relative humidity to 0.0, the composites were exposed to a desiccant (Drierite), that depleted the system of any moisture. To accomplish a relative humidity of 1.0, pure water was placed in a dish alongside the dish of composites. The saturated salt solutions made for this study are shown in Table 3.1.

Table 3.1. Measured relative humidities of varying salt solutions used in this experiment.

Saturated Salt	Relative Humidity (Measured)
Potassium Acetate	0.225
Potassium Carbonate	0.432
Sodium Chloride	0.746
Potassium Chloride	0.845
Potassium Chromate	0.865
Barium Chloride	0.902
Copper Sulfate	0.973

After the relative humidities were set, the experiment proceeded. The only variable in the system was the length of time in varying relative humidities. This meant the change in weight of the tablet was only due to water condensation in the composite's nanoscale cracks. It is known that water condenses in small pores before large pores. An equilibrium

is reached in different sized pores, dependent on the relative humidity. This relationship can be described by the Kelvin-Laplace Equation (Eqn. 3.1),

$$a = \frac{2\gamma \cos \theta}{(RT/\bar{V}_L)\ln(p/p_0)}$$

(Eqn. 3.1)

where a is the maximum pore radius that can be filled at a given vapor saturation ratio, γ is the liquid/vapor surface tension (73 mJ/m^2), θ is the contact angle (0 assuming perfect wetting), R is the gas constant (8314.5 mJ/Kmol), T is the temperature (298 K), $\bar{V}_L$ is the specific volume (0.001 m^3/kg), and p/p_0 is the vapor saturation ratio, or relative humidity. From this relationship, it was possible to infer a pore radius range for each relative humidity. This was accomplished by, first, calculating the maximum pore radius filled for a given relative humidity that a composite is exposed to. Because pores fill from small to large, it was possible to generate a range of filled pores for each given relative humidity. For example, if a composite is exposed to a relative humidity of 0.43, pores with radii 1.26 nm and smaller will be filled. If a composite is exposed to a relative humidity of 0.75, the maximum pore size filled is 3.74 nm. However, we do not know the exact sizes of pores within our system. There may not be any pores with a radius of 3.74 nm. Thus, a range of possible maximum sizes was established for each given relative humidity. For the example of 0.75, water condenses in all pores up to a radius of between 1.26 nm and 3.74 nm. This range generation, done for all relative humidities, is shown in Table 3.2.

Table 3.2. The maximum pore radius filled at a given relative humidity, and the range of these pore sizes given varying relative humidities.

p/p_o	a (nm)	Range max pore size (nm)
0	0.00	
0.225	0.77	0-0.77
0.432	1.26	0.71-1.26
0.753	3.74	1.26-3.74
0.843	6.23	3.74-6.23
0.865	7.32	6.23-7.32
0.903	10.40	7.32-10.40
0.972	37.38	10.40-37.38

A log-log plot of the data collected was generated, shown below in Figure 3.2. The plateaus suggest the pores were saturated, and the difference in mass between the plateaus, Δm, was used to calculate the change in water volume condensing in pores, since volume is proportional to mass. This plot also provided the time needed to saturate the pores at varying relative humidities, $t_c \approx 20$ hours. Thus, experiments were planned around exposing composites to different relative humidities for at least 48 hours to ensure the pores were fully saturated. Additionally, the slope of these lines in the range $0\,\text{h} \leq t \leq 20\,\text{h}$ is about 0.5, which suggests that the condensation process is diffusion-limited.
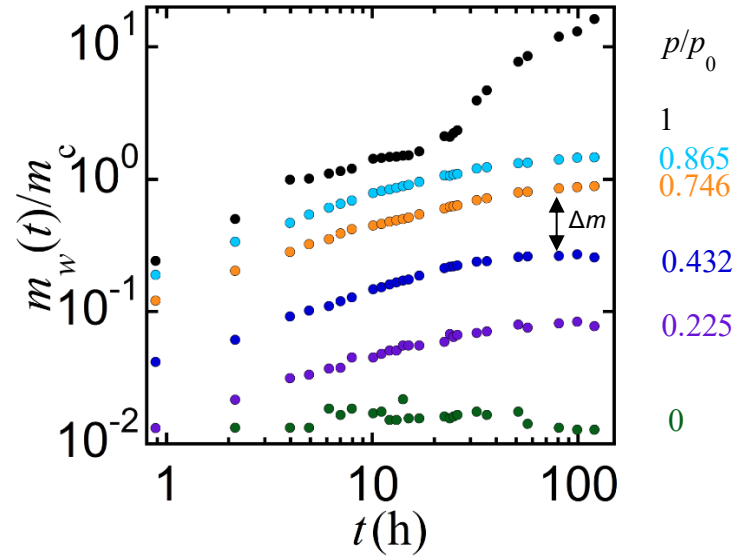
Figure 3.2. Log-log plot of weight percent increase of the tablet versus time, of imbibed tablets kept at different relative humidities over the span of 100 hours. The plateaus suggest saturation of the tablets, and the difference between plateaus is indicative of the difference of mass changes, Δm. The 1.0 relative humidity composite indicates breakup.

The volume changes, proportional to mass changes, associated with different relative humidities, along with the pore size range for each relative humidity (Table 3.2) are coplotted to illustrate the pore size distribution in the imbibed tablet. This plot is shown in Figure 3.3.
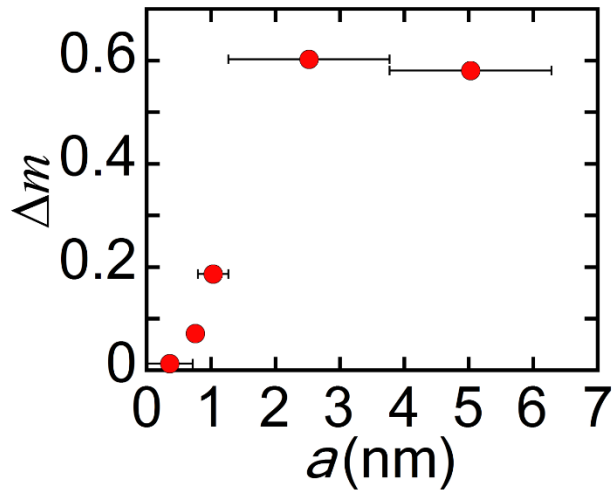
Figure 3.3. The distribution of pore sizes in an imbibed tablet, using the volume of occupied pore space associated with different relative humidities, Δm, and the average of pore range associated with each relative humidity. The standard deviation bars illustrate the upper and lower limits on the maximum pore size.

A large pore will of course contain more water than a small pore; thus, the plot above suggests that the distribution is dominated by large pores. To provide a distribution that illustrates the number of pores of a given size, the volume change was normalized by dividing the mass at each point by the associated radius cubed, $\Delta m/a^3$. This generated a pore frequency distribution, and is shown below in Figure 3.4., where the large vertical standard deviation bars are derived from the uncertainty associated with dividing Δm by the lower and upper pore range values. The normalized pore size distribution above fits a log-normal distribution. Pores with a radius of about one nanometer are most frequent, while pores with a large radius of about five nanometers are sparser. Pores between two and three nanometers are semifrequent, but it is important to notice the broad range of maximum pore size associated with this data point.
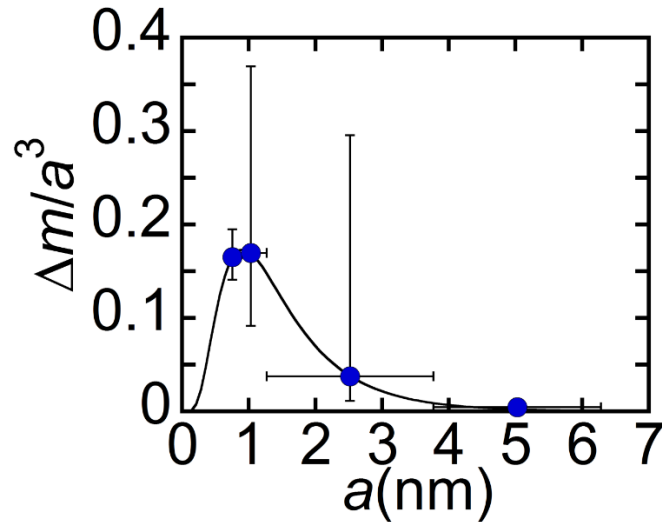
Figure 3.4. Normalized plot of data shown in Figure 3.3, illustrating the normalized volume versus the maximum pore radius. This log-normal distribution shows the frequency of pores with a given diameter, *a*, in a composite.

The distribution of pore sizes was important to obtain to analyze the effects relative humidity has on a composite. Equilibrium logic implied that imbibed tablets at a lower relative humidity have less condensed water in their pores than those at high relative humidities. Lower relative humidities have less water available to interact in the condensation-evaporation exchange. A lower relative humidity means, by definition, there is a lower associated vapor pressure, which implies equilibrium may be obtained faster. Interestingly, this is not a phenomenon that is clearly observed. This implies that the difference in rate of equilibrium, via condensation, happened faster than the sampling time interval.

This quantitative study successfully demonstrates the existence of nanoscale cracks in the composite that permit water to enter the composite. The implication of water within the composite supports the hypothesis of the generation of a supersaturated solution allowing for the growth of crystals.

After the quantification of nanoscale cracks in composites, new composites were subjected to the previous protocol. After 72 hours of exposure to varying relative humidities, the composites were dropped in water and breakup was recorded. This was done to detect any qualitative impact exposing composites to different relative humidities has on breakup intensity. It was observed that breakup became drastically less dramatic as imbibed tablets were subjected to higher relative humidities. The last image, a composite held at a relative humidity of 0.97, shows a large crack. This crack existed before the composite was dropped in the water. In other words, dropping this composite in water did not have any effect on the mechanical integrity. The difference in breakup intensity is shown in Figure 3.5.

Figure 3.5. Images taken five minutes after imbibed tablets, at different relative humidities for three days, were placed in water. Images are in order of increasing relative humidity left to right, by row: 0.225, 0.432, 0.746, 0.865, 0.902, 0.973.

The decrease in breakup intensity shown in Figure 3.5 may be because as relative humidity is increased, more void pore space is occupied by condensation. At low relative humidities, large pores remain water vacant, since pores fill small to large. When these

composites are then placed in water, the medium and large pores fill with water, mobilizing drug and create a supersaturated solution. This supersaturated solution drives crystal growth, and the pressure exerted by the crystals on the silica causes breakup. There are less vacancies in composites exposed to higher relative humidities. This means that more pore sizes have been filled with water due to condensation, and have thus generated a supersaturated solution and generated crystal growth. This growth may be enough to break the composite apart, as seen in the case of a composite at a relative humidity of 0.973. When the sparse, as seen in Figure 3.4, large pores fill with water when dropped in water, they too generate a supersaturated solution. However, due to their infrequency in the system, do not collectively generate enough pressure via crystal growth to exceed the yield strength of the silica. This coincides with the idea that generating a supersaturated solution in the largest pores may not generate a pressure large enough to break the composite.

To explore this hypothesis, an experiment was developed around exposing a composite to a relative humidity of 1.0. If the previous hypothesis is correct, crystals will grow when the composite is placed in a humidity of 1.0 and crack the composite. When placed in water, there should be no growth as all pores are filled with grown crystals and water. When some of the water in the pores is driven off due to a pressure change induced by exposed the composite back to a relative humidity of 0.0, there should be minimal breakup in water. Additionally, when exposed to a relative humidity of 1.0, the pores should fill completely and thus no longer act as a water transport system.

A composite was exposed to a relative humidity of 0.0 for 24 hours and placed in water. Breakup is observed. A composite is then placed in a relative humidity of 0.0 for 24

hours then 1.0 for 24 hours, and finally placed in water. This is enough time (as shown in Figure 3.2) to saturate the pores within the composite. This saturation induces a supersaturated solution and crystals grow, cracking the composite. When the composite, with filled pores, is placed in water there is no longer a transport network and water cannot enter the composite. Thus, crystal growth doesn't occur as a result of being placed in water. If we take a new composite and expose it to the same regimen as the previous one, but place it back in a relative humidity of 0.0 for 24 hours before dropping it in water, we drive off some of the water in the pores. The change in relative humidity causes a pressure change and water evaporates from the pores. However, crystals have already grown because of the supersaturated solution generated when placed in a relative humidity of 1.0. Thus, when placed in a dish of water, only minimal crystal growth happens. That is, the water reenters the vacant large pores and generates another supersaturated solution, but the crystals are less inclined to grow, as they have already grown in a way to reduce their surface energy (the driving thermodynamic force for crystal growth as discussed extensively in the following chapter). This means only minor crystal growth is occurring, which is reflected in the minimal breakup, or swelling, of the composite in water. Experimental results from this experiment are shown in Figure 3.6.
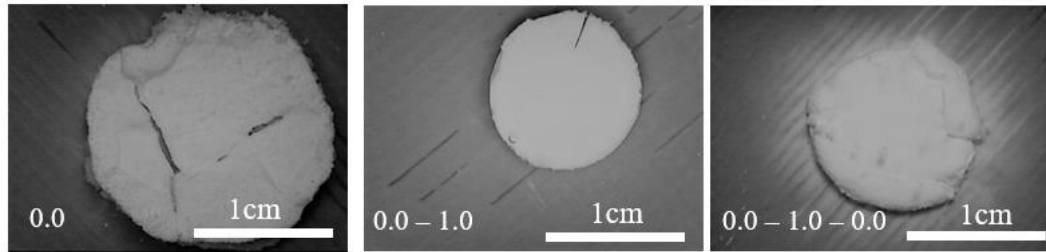
Figure 3.6. Imbibed tablets subjected to 0.0 and 1.0 relative humidities for 24 hours at a time, then dropped in water. All images were taken five minutes after the tablets were placed in the water.

To test the hypothesis that water does not transport through a composite held at a relative humidity of 1.0, a composite was subjected to the previous protocol and placed in food coloring diluted 1:2. Another composite was subjected to a relative humidity of 0.0 for 24 hours, then placed in food coloring diluted 1:2 as a control. The result from the experiment is shown in Figure 3.7, illustrating that water does not appear to transport through a composite kept at relative humidity of 1.0 failing to disprove our hypothesis.
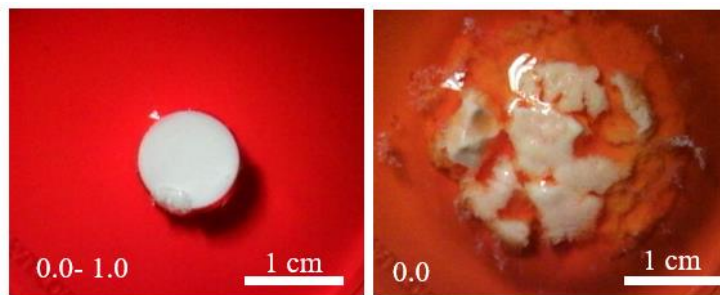

Figure 3.7. A composite placed in a relative humidity of 0.0 for 24 hours, 1.0 for 24 hours, then into a 1:2 solution of food coloring and water, shown on the left. A composite placed in a relative humidity of 0.0 for 24 hours then into a 1:2 solution of food coloring and water is shown on the right. Both images are taken five minutes after being placed in the 1:2 solution of red food coloring and distilled water, and illustrate the lack of solution transported through the composite held at a relative humidity of 1.0.

Studying the microstructure of nanoscale cracks in the composite results in the conclusion that they act as a transport system for water through the composite. This

quantification of nanoscale cracks supports the hypothesis that a supersaturated solution may exist in the composite, composed of water and drug. To understand the impact that this supersaturated solution has on crystal growth in the composite, Differential Scanning Calorimetry (DSC) is conducted.

CHAPTER FOUR

DIFFERENTIAL SCANNING CALORIMETRY

Differential scanning calorimetry (DSC) measurements were performed on drug-silica composites to quantify two parameters: (1) the fraction of crystal drug content and (2) the drug crystal size distribution. DSC is a thermoanalytical method that measures the heat necessary to raise the temperature of a sample, as a function of temperature.[13] This technique can measure many characteristics of a sample such as heat capacity, glass transition, as well as the temperature and latent heat associated with a phase transition.[13] The heat capacity of a sample is given by the slope of the generated plot, heat flow versus temperature.[13] Phase transitions are indicated by the relative difference in heat flow needed to keep the temperature of a sample and reference equal. For example, when a sample undergoes an exothermic process such as crystallization, less heat is required to raise the sample temperature than the reference. Likewise, when a sample undergoes an endothermic process such as melting, it absorbs heat, and the system must increase the heat flow to the sample pan to keep the temperature of the sample and reference pans equal.

Measuring the temperature and latent heat associated with the melting of drug in our composite was critical for determining the phenomenon responsible for composite breakup. The drug is solid at room temperature, so when heat is applied we expect it to melt. The area under the concave, endothermic, DSC curve allowed us to calculate the amount of crystalline drug in the composite. Changes in melting temperature provide

insight to the size of the crystal confined by the pores, as larger crystals melt at higher temperatures.

To calculate the crystal and amorphous content of drug in the composite, two parameters must be known: (1) the enthalpy of melting (heat of fusion) for a pure crystalline sample $\Delta H_{m,\text{pure}}$, and (2) the mass fraction of the sample occupied by the organic drug, m_c. With this information, as well as the enthalpy associated with the sample of interest $\Delta H_{m,\text{sample}}$, it was possible to calculate the fraction of crystalline drug φ_c in a given sample using the following equation.

$$\varphi_c = \frac{\Delta H_{m,sample}}{m_c \Delta H_{m,pure}} \qquad \text{(Eqn 4.1)}$$

To determine m_c, thermogravimetric analysis (TGA) is used. TGA uses a highly sensitive scale to monitor the mass of the composite as a function of temperature. At temperatures above 150°C, the organic drug in the tablet begins to oxidize and degrade and will be released as carbon dioxide and oxygen; by contrast, the inorganic silica does not degrade at these temperatures. Thus, the corresponding decrease in mass can be used to determine the mass fraction of drug in the original sample. A representative measurement is shown below in Fig. 4.1 for a fenofibrate-silica composite, providing $m_c = 0.182$.
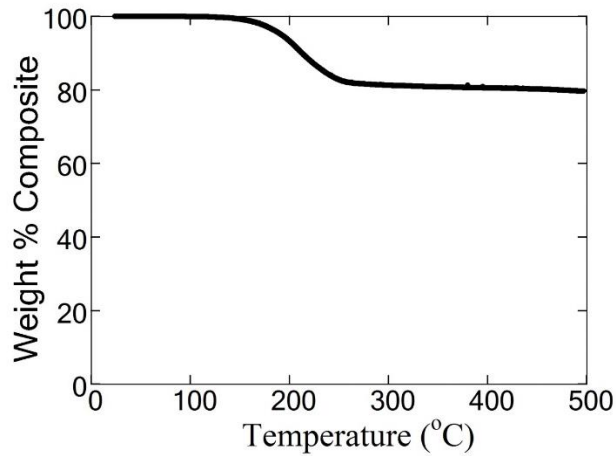
Figure 4.1. Thermogravimetric analysis (TGA) plot of mass as a function of temperature for a fenofibrate-silica composite heated to 500°C at a ramp rate of 3°C/min. The fenofibrate occupies about 18% of the tablet by weight.

To determine $\Delta H_{m, pure}$ for fenofibrate, as well as to establish a benchmark, DSC measurements were performed on pure fenofibrate powder. DSC measurements were performed on three independent samples. For each measurement, a sample of known mass was placed in a hermetically sealed pan alongside an empty reference pan. Each pan was placed on a pedestal that records the amount of energy required to keep both the reference and sample pan at the same temperature. All DSC runs were conducted with a heat ramp rate of 1°C/minute, starting at ambient temperature. A representative DSC measurement is shown in Fig. 4.2. The melting point, T_m of the pure drug was measured to be 80.2 ± 0.05°C, with $\Delta H_{m, pure} = 31.52 \pm 0.37$ kJ/mol. These results are consistent with the published values of $T_m = 80.5$°C and $\Delta H_{m, pure} = 32.4$ kJ/mol, with percent differences of about 0.37% and 2.75%, respectively.[14]
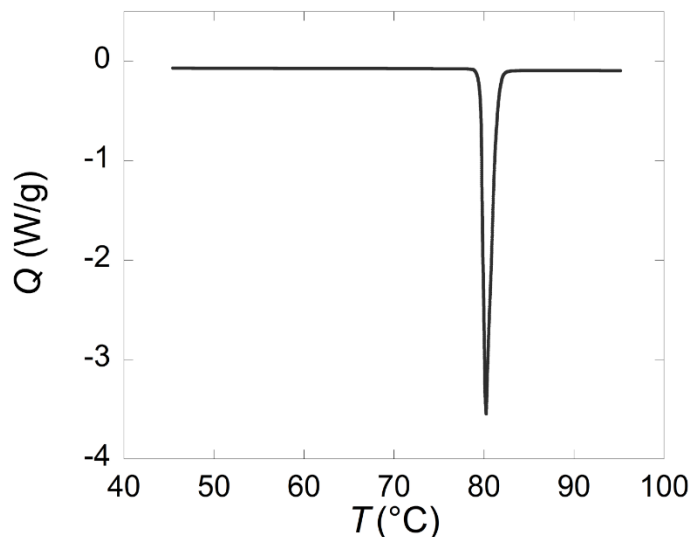
Figure 4.2. Differential scanning calorimetry (DSC) plot of relative heat flux Q as a function of temperature T for pure fenofibrate, heated at a rate of 1°C/min. The plot is the average of three runs and the standard deviation is smaller than the symbol size. These results yielded an average melting temperature of $T_m = 80.2 \pm 0.05$°C and average heat of fusion of $\Delta H_{m, pure} = 31.52 \pm 0.37$ kJ/mol.

To determine the crystalline content of drug in the composite and the drug crystal size distribution, both as a function of relative humidity, samples were prepared as described in Chapter 2. Following imbibition, samples were immediately transferred to a low humidity chamber ($p/p_0 = 0$) for 24 hours. After 24 hours, the composites were transferred to different relative humidities of 0.0, 0.25, 0.43, 0.75, 0.84, 0.86, 0.90, 0.97, and 1.0 for three days. They were removed from the respective relative humidity chambers and moved back into the low humidity chamber for an additional three days to drive off the water that condensed in the pores during residency in humidity chambers. This was done as the presence of water would adversely affect the DSC results. It was assumed that changes resulting from the condensation of water are permanent and unaffected by the removal of the condensed water prior to the DSC measurements. To perform DSC

measurements, samples were meticulously weighed and sealed in hermetic DSC pans. Samples were then transferred into the DSC. A program was constructed in TRIOS to dictate the experimental protocol. All samples were run starting at a temperature no higher than 35°C, with a ramp rate of 1°C/minute up to 95°C. Results from this experiment are shown in Fig. 4.3.
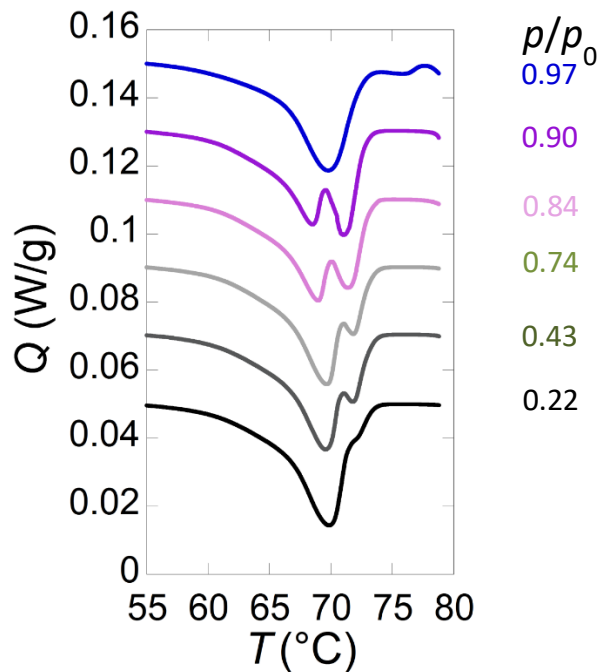

Figure 4.3. Differential scanning calorimetry (DSC) results of imbibed tablets that were subjected to different relative humidities, p/p_0 for three days. Two aspects of the data should be noted: (1) the integrated areas associated with these curves are proportional to the fraction of drug in crystal form, and (2) the melting point depression can provide crystal size. Data plots are offset for clarity.

To calculate the crystalline content of drug in the composite from the DSC curves in Fig. 4.3, the integrated area associated with each curve are measured with the TRIOS software and Equation 4.1 was used to calculate the fraction of crystalline content in the composite as a function of relative humidity. Surprisingly, there were minimal changes in

the percent crystallinity with varying relative humidity, as shown in Fig. 4.4. This suggested that the overall amount of drug crystallized in each tablet did not change significantly with the condensation of increasing amounts of water, leading even to breakup. Thus, our hypothesis of amorphous drug feeding the crystal growth of crystalline drug was not supported by the DSC results.
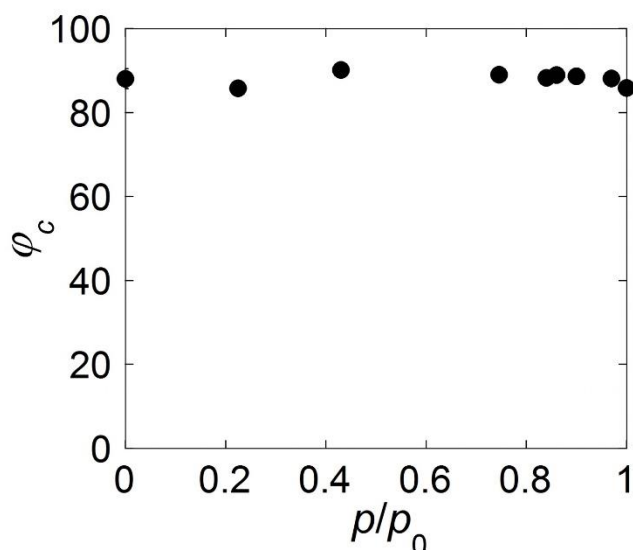

Figure 4.4. Mass fraction of drug in crystal form φ_c calculated for each tablet kept in varying relative humidities, p/p_0. Three trials are conducted, and the mean is shown here with standard deviations smaller than the symbol size. This figure shows that percent crystallinity does not change with the induction of water into the composite.

To determine the evolution of the crystal size distribution with p/p_0 the Gibbs-Thomson equation was used. The Gibbs-Thomson equation which follows states that melting point depression ΔT is inversely proportional to crystal size, where d is the diameter of the crystal.

$$\Delta T = \frac{4\lambda_{sl}T_{m,b}}{\Delta H \rho d} \qquad \text{(Eqn 4.2)}$$

Here, λ_{sl} is the interfacial tension, $T_{m,b}$ is the melting temperature of large drug crystals, ΔH is the heat of fusion of the crystalline drug, and ρ is the drug density. To highlight this melting point depression effect, DSC runs of the composite and large fenofibrate crystals are plotted in Fig. 4.5.
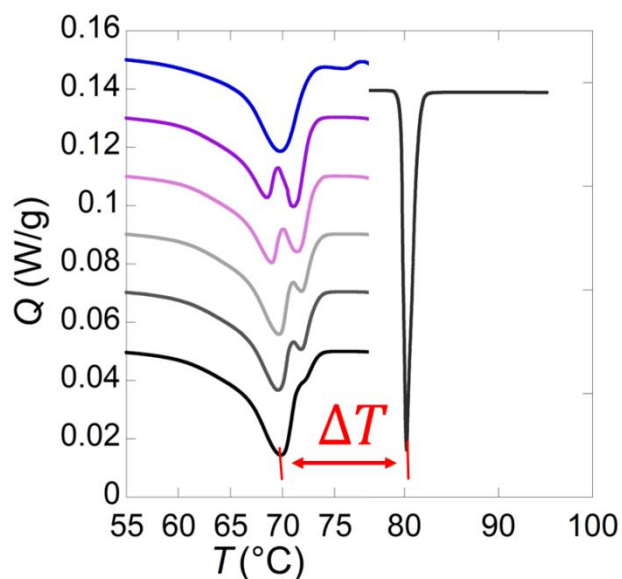

Figure 4.5. The melting point depression, ΔT, as used in the Gibbs-Thomson equation. This melting point depression refers to the difference between the melting point of large (macroscale) fenofibrate crystals and our composite samples. Data plots are offset for clarity.

To utilize the Gibbs-Thomson equation, the most straightforward approach was to systematically vary drug crystal size and construct a calibration plot. To do this, we used templating silica spheres of varied sizes to construct porous media with different sized pores. It has been demonstrated mathematically that the maximum sized sphere that can fit in a two-dimensional pore formed by three "kissing spheres" is approximately 15% of the diameter of the larger spheres. For example, the maximum size sphere that can fit into a pore formed by colloidal silica with $D = 100$ nm is 15 nm. However, based on TEM images

taken at Harvard University by Esther Amstad, the average crystal size in a porous material composed of colloidal silica with $D = 100$ nm is 9 nm. Thus, the calibration curve was constructed using the following relationship.

$$d = 0.09D \qquad \text{(Eqn. 4.3)}$$

Fenofibrate-silica composites were made using four varied sizes of colloidal silica, DSC measurements were performed on each, and the melting point depression ΔT was measured for each and plotted against the inverse maximum diameter of crystal d based on Equation 4.3. The resulting plot, fit with a straight line is shown in Figure 4.6.
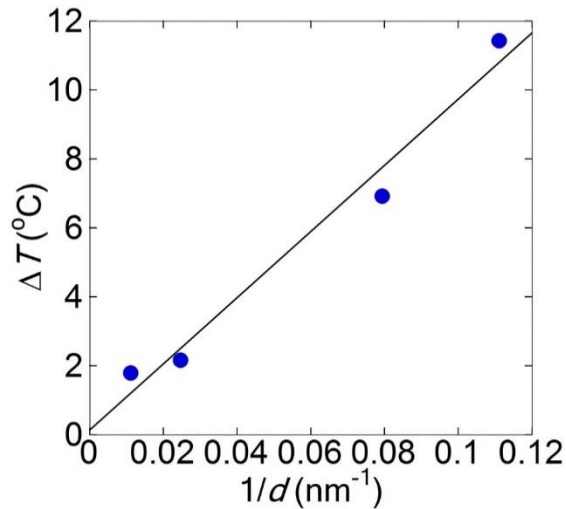
Figure 4.6. Melting point depression ΔT as a function of the inverse of crystal size, d. Data was extracted from DSC measurements on fenofibrate-silica composites made using four different sizes of colloidal silica and the crystal size based on the relationship: $d = 0.09D$.

To plot the calibration curve in an alternative manner, the melting point of the crystals in the composite was plotted as a function of the inverse of the crystal size, d as shown in Fig. 4.7.

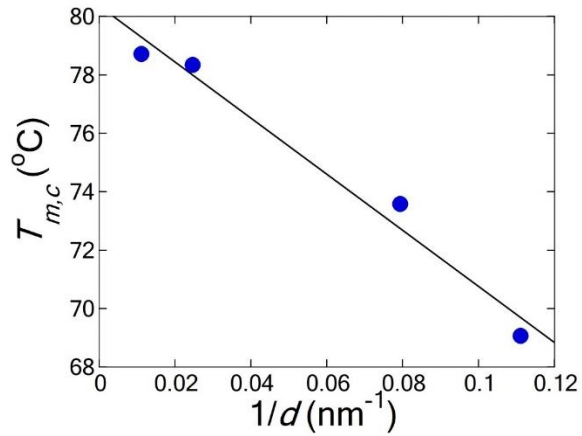Figure 4.7. An adjusted calibration curve of the melting point of crystals see in DSC plots as minima, and maximum diameter of crystal confined in a pore provided by silica beads.

The calibration curve was then used to convert each DSC plot to a crystal size distribution. Each melting temperature is directly related to the diameter of crystal, so the x-axis was directly converted from temperature to crystal diameter. In addition, heat flux is directly proportional to the mass of crystals at a given size; so, by simply multiplying Q by -1, the y-axis was converted into arbitrary units of intensity. This provides the evolution of the crystal size distribution with respect to relative humidity. We observed several striking phenomena. At low humidities, the crystal size distribution is peaked around a single crystal size ($d \approx 8$) with a slight shoulder ($d \approx 11$). As the composites were exposed to greater humidities, the shoulder grew into a clear peak and shifts to larger size. This is plotted in Fig. 4.8.
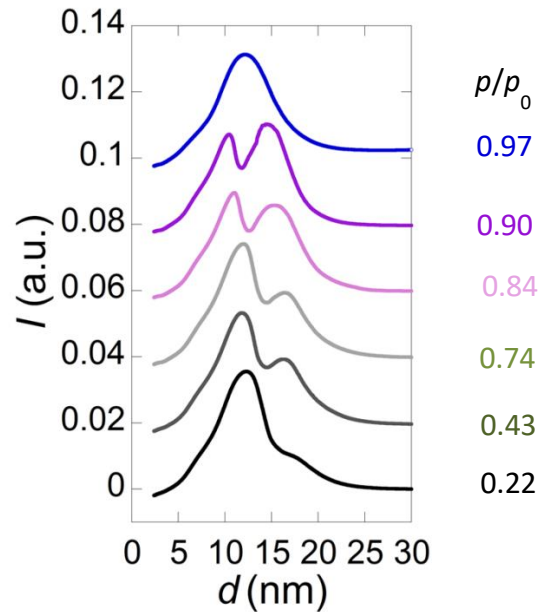
Figure 4.8. DSC data from Fig. 4.5 after conversion to a crystal size distribution. Each curve represents the mean of three DSC runs. Deviation in the data is less than the symbol size. Data plots are offset for clarity.

To more clearly understand the evolution of crystal size with relative humidity, we plot the primary peaks in the size distribution with respect to relative humidity. This data is shown in Fig. 4.9. where the left-most peak is represented with red symbols, and the right-most peak is represented with blue symbols. The data implied that the composite breaks when placed in a relative humidity above 0.93. This agreed with observations made during the experiment and suggests that a redistribution of crystal sizes could be the driving force for breakup.
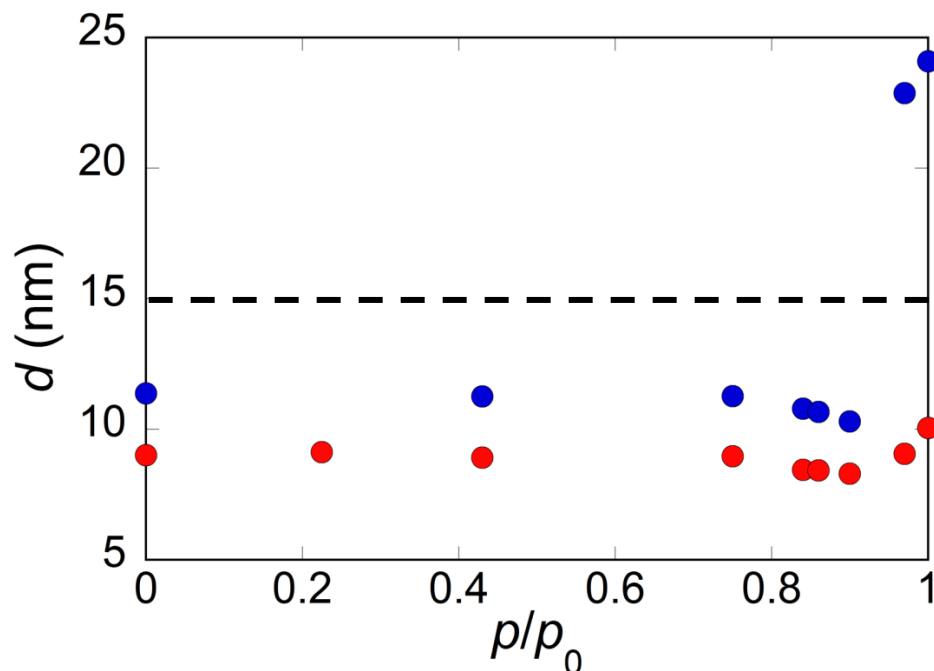
Figure 4.9. Plot of the primary peak position as a function of relative humidity. It shows that the crystal size increases with the induction of more water. The dashed line represents a threshold: the maximum size of a spherical crystal that could fit in a pore provided by silica beads with $D = 100$ nm. When the crystal grows larger than the pore size, breakup is expected.

The DSC data shows that larger crystals are growing at the expense of smaller crystals. This phenomenon is known as Ostwald ripening and is typically associated with coarsening behavior in emulsions and other colloidal systems; however, this phenomenon could also generate the supersaturation necessary for crystal pressure and drive composite breakup.[15]

To understand how Ostwald ripening could create a supersaturation, consider two nanoscale crystals: one slightly larger than the other (Fig. 4.10a). Initially, the crystals are dry, and are then immersed in water (Fig. 4.10b). Based on equilibrium thermodynamics, when the crystals come in contact with water, they dissolve until they reach equilibrium

saturation. The saturation solubility of nanoscale crystals is described by the Ostwald-Freundlich equation, which relates the equilibrium saturation solubility associated with a particle, C_r to the radius of the particle, r.

$$\rho \frac{RT}{M} ln \frac{C_r}{C_\infty} = \frac{2\gamma}{r} \qquad \text{(Eqn. 4.4)}$$

Here, ρ is the drug density, R is the gas constant, T is temperature, M is molar mass, C_r is the solubility of a particle with radius of curvature r, C_∞ is the solubility of a particle with a very large radius of curvature, and γ is the interfacial surface tension. From this relationship, it is clear the smaller the crystal, the greater the equilibrium saturation solubility ($C_{sat,S} > C_{sat,L}$). This means that as both crystals continue to dissolve, the larger crystal will reach equilibrium saturation before the smaller crystal. Meanwhile, the smaller crystal will continue to dissolve as long as $C_{drug} < C_{sat,S}$. As a result, the solution will become supersaturated with respect to the large crystal ($C_{drug} > C_{sat,L}$). If the scenario depicted in Fig. 4.10a-e occurs within the confines of a pore, the supersaturation generated by the smaller crystal could provide the conditions necessary for the larger crystal to exert a pressure on the pore walls, as shown by the series of illustrations in Fig. 4.11.
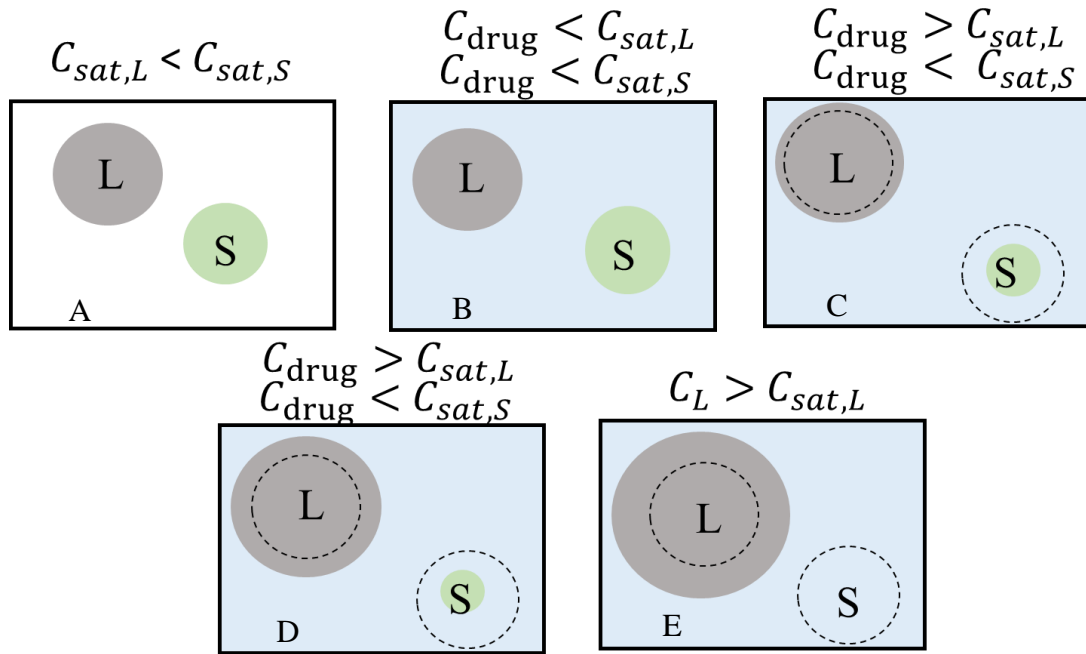
Figure 4.10. (a) Ostwald ripening of crystals in water. Consider two nanoscale crystals: one large, L and one small, S. (B) When the pore is filled with pure water, the concentration of drug in the water will be less than the solubility of both the large and small crystals. (C) As both crystals dissolve, the larger crystal will reach equilibrium saturation before the smaller crystal. The continued dissolution of the smaller crystal will generate a supersaturated solution with respect to the large crystal and will drive growth of the larger crystal (D, E).
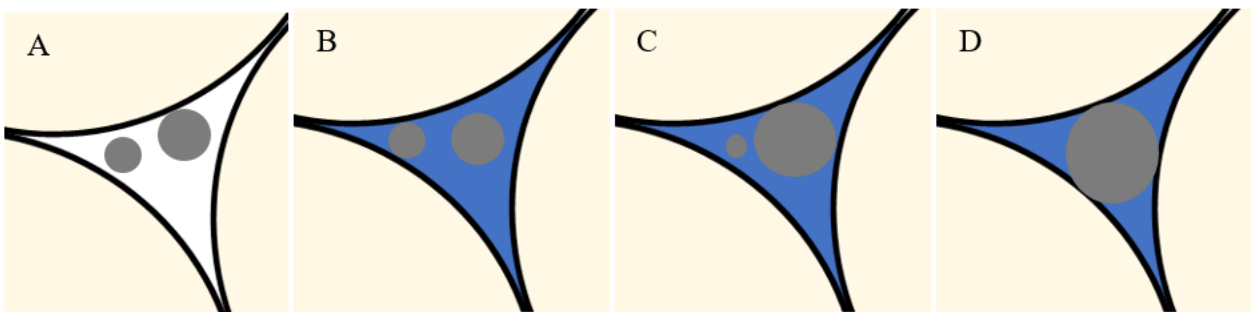

Figure 4.11. Ostwald ripening of crystals within a pore provided by silica spheres. (A) Heterogenous crystallization of fenofibrate would likely lead to a distribution of crystal sizes in the composite. (B) Once the pores are filled with water, the Ostwald ripening phenomenon described in Fig 4.10 could result in a pressure being exerted on the walls of the pore (C, D).

In the same manner, crystal pressure could also be generated by the growth of deformed crystals.[16] For example, consider a cylindrical crystal with two spherical ends, confined by a cylindrical pore (Fig. 4.12A). The spherical caps have a greater mean curvature than the central cylindrical portion of the crystal; thus, according to the Ostwald-Freundlich equation, the caps will have a higher saturation solubility than the cylindrical center ($C_{sat,caps} > C_{sat,center}$). This means that if the crystal is immersed in water, the central region will reach equilibrium saturation before the spherical caps. However, the caps will continue to dissolve as long as $C_{sat,caps} < C_{drug}$. As a result, the solution will become supersaturated with respect to the cylindrical region of the crystal ($C_{drug} > C_{sat,center}$). If the scenario depicted in Fig. 4.12a-e occurs within the confines of a pore, the supersaturation generated by the deformed crystal could provide the conditions necessary for the larger crystal to exert a pressure on the pore walls, as shown by the series of illustrations in Fig. 4.13. Due to the non-spherical nature of the pores in the composites, it is very likely that deformed crystals are indeed forming in the pores.
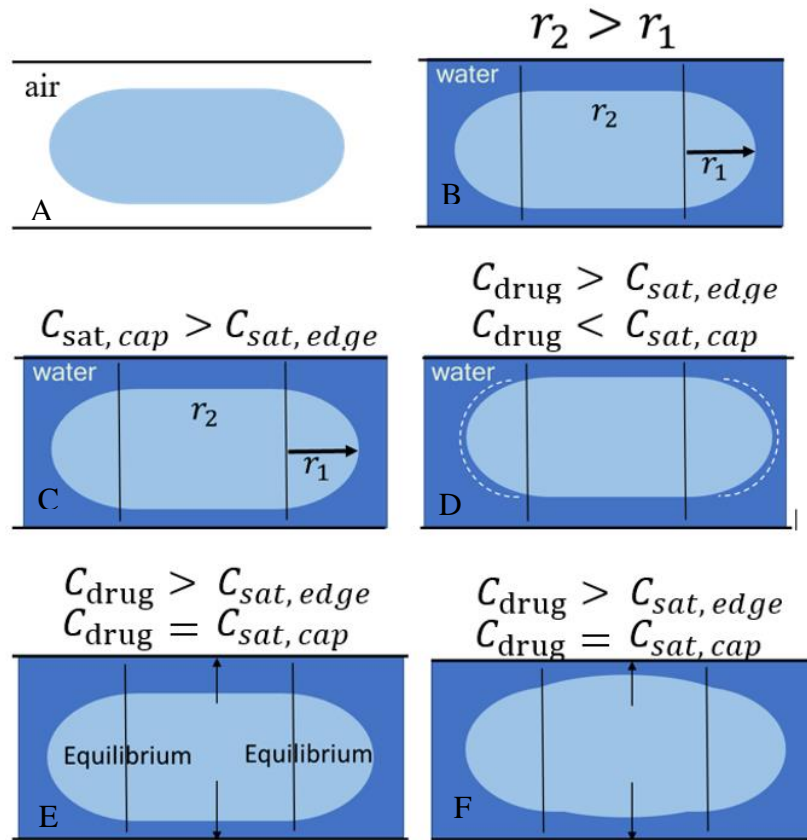
Figure 4.12. A deformed crystal redistributing its mass to minimize surface energy, leading to pore breakup. A deformed crystal exists in a non-spherical pore (A). Due to the difference in radii of the planar edges and spherical caps, the solubility of the edges is less than the caps (B, C). The caps dissolve until they are in equilibrium with surrounding solution (D, E). Because the concentration of drug in the solution is greater than the solubility of the planar edge, it is a supersaturated solution (D, E). This leads to the growth of the planar edges at the expense of the spherical caps (F).

Figure 4.13. A deformed crystal in the pore space provided by the colloidal silica redistributes its mass to minimize surface area, and thus surface energy (A). The spherical caps, with a smaller radius of curvature thus larger so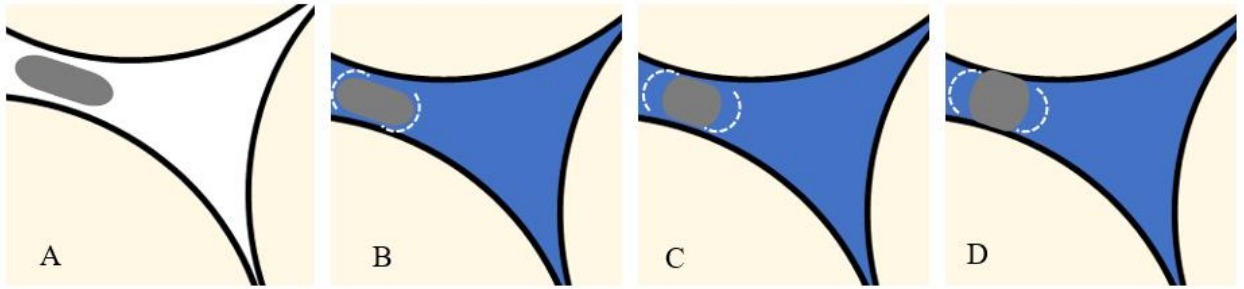lubility, dissolve in water more than the planar regions (B). The planar region is then in a supersaturated solution as the concentration of drug in the water exceeds the solubility of the flat surface, and grows outward (C). The growth of the planar regions on the walls of the silica applies a pressure that eventually overcomes the yeild strength of the composite, due to growth exceeding the size of pore (D).

It is entirely possible that both Ostwald ripening and rearrangement of deformed crystals are happening simultaneously within pores. The DSC data implies there are at least two definite crystal sizes present in the pores, but there are likely many more. This is suggested by the slow decent into the melting point of a confined drug, easily seen when compared to the sharp melting point peak in the unconfined drug curve. Multiple crystals could be simultaneously rearranging to minimize their surface energy, while also playing a role in multi-crystal Ostwald ripening. This dynamic and complex system may be responsible for the ultimate failure of the mechanical integrity of the composite.

APPENDICES

APPENDIX A

PRELIMINARY H-NMR DATA

Proton Nuclear Magnetic Resonance (H-NMR) was used to analyze crystallization mechanics, with respect to relative humidity changes, over time. All scans and data construction were done by Linn Thrane, a Ph.D. candidate working in the lab of Dr. Joseph Seymour at Montana State University. Data analysis was done in collaboration with Linn Thrane, Dr. Seymour, and Dr. Wilking. H-NMR was conducted for pure drug, not imbibed in a tablet, to understand if the local physical and chemical environment changes when compared to drug confined in the pores of a tablet. The composites used in this study were made from colloidal silica (SiO_2) imbibed with fenofibrate ($C_{20}H_{21}ClO_4$). Composites were tested after water (H_2O) condenses inside void pore space of the composite. It is obvious from the molecular formulas that the only entities measured using H-NMR were the drug and water in the pores, as H-NMR measures hydrogen nuclei in molecules.

T_1 and T_2 relaxation times were obtained for the restricted and unrestricted drug. Two plots were generated: a probability plot of T_2 relaxation times, as well as a log-log plot of T_1 versus T_2 relaxation times. A T_2 probability versus log T_2 plot lead to deductions about drug mobility in pores, as well as relative quantities of chemical entities within the tablet. Once in the magnet, every individual molecular spin experiences a different magnetic field. This is a consequence of intermolecular interactions; that is, the neighboring influences lead to an eventual dephasing of spins. This dephasing leads to a signal reduction over time, or T_2 relaxation time.[17] Molecules confined in pores interact with and influenced neighboring molecular spins more than less restricted molecules. This increased interaction leads to longer T_2 relaxation times. Drug that is in an amorphous state has more mobility than its crystal counter structure, and thus a longer T_2 time is expected.

Additionally, pure unimbibed drug is expected to have a longer T_2 time than imbibed drug, due to pore restriction.

The T_1T_2 plots served to verify the experimental method, track molecular arrangements of populations within the tablet, and indicated whether the sample was more or less solid-like. When a magnetic field is applied to the sample, the molecules are forced into a perpendicular orientation (from the *z*—axis to the *x*—axis). T_1 relaxation times are a measure of how long it takes for the molecules to reorient into the z-axis after the magnetization is removed.[17] When analyzed alongside T_2 relaxation times, information about the physical state of the sample was revealed. A short T_2 time along with a long T_1 time indicated a more solid-like substance, while a long T_2 and T_1 time implied a more liquid-like substance. This information was used to gather data about the conversion of a more liquid-like amorphous drug to a more solid-like, or crystalline, structure.

To understand the timescale of crystallization of drug in the pores because of imbibition, pure drug was melted in an NMR tube then placed in the magnetic and measured. Specifically, a 5 mm NMR tube (Wilmad Economy) was filled with pure fenofibrate, straight from the bottle received from TCI. After being filled to 90% capacity, the tube was placed in an oven at 90 ºC until melted. The tube was then quickly capped and transferred into the magnetic, when the analysis begun. Measurements were taken every three minutes at ambient conditions. This interval was chosen to maximize data collected while minimizing noise via multiple scans per data point. Data from this experiment is shown in Figure A.1.
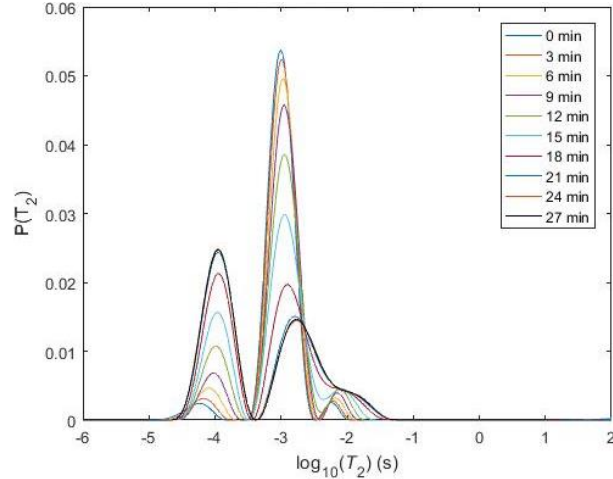
Figure A.1. T_2 H-NMR scans of pure fenofibrate recrystallizing after being melted. This illustrates the time scale of crystallization of the drug, as well as conformational changes from primarily amorphous to primarily crystalline content.

Figure A.1 shows equilibrium was acquired, due to the lack of signal variance, after about 21 minutes after melting. This illustrated the evolution from being completely amorphous to mostly crystalline. The longer T_2 time of the right-most peak implied a more mobile population, indicative of amorphous content. Contrarily, the shorter T_2 time of the left-most peak implied a less mobile population, indicative of crystalline content. The peak with the longer T_2 diminishes over time, while the other peak seems to increase in intensity. This observation implies a growing crystalline population and shrinking amorphous population. Due to the conservation of mass, it is logical to assume that the amorphous content evolved into crystals as a function of time. This supports our hypothesis of drug crystallization post imbibement.

To explore this hypothesis further, an analysis of crystallization over time was conducted on drug in a tablet. Three silica templates, all slip casted in the way previously described, were cut into pieces small enough to fit into an NMR sample tube. Once

fenofibrate was melted on a hot plate at 90°C, the silica template fragments were placed on top. After the pieces turned clear, indicating imbibition was complete, the pieces were taken off the hot plate and wiped clean with a tissue. The clean pieces of tablet were transferred into a NMR sample tube and loaded into the magnet promptly. Scans were initiated immediately. Scans of the evolving tablet pieces were taken every 15 minutes until there was no variation in the T_2 relaxation times and intensities, about 27 minutes. Results from this experiment are shown as follows in Figure A.2.
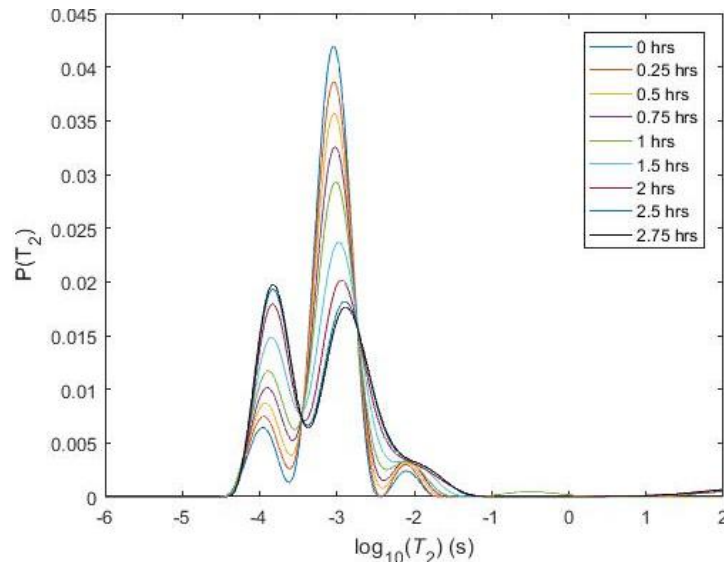

Figure A.2. T_2 H-NMR scans of drug recrystallizing inside the porous silica, immediately after imbibition. This plot shows the evolution of amorphous to crystalline drug, within a time scale of two and a half hours.

Figure A.2. clearly illustrates the evolution of amorphous to crystalline drug, like the previous figure. It is evident from this data that drug crystallization happens over, about, two and a half hours. As expected, crystallization happened more slowly when confined in pores than when unconfined as in the previous plot. The intensity of the two peaks equalize, implying an equilibrium state of amorphous and crystalline content. Similar to the pure,

powder drug previously, it is hypothesized that the amorphous content is evolving into crystals inside the silica pores.

Many experiments conducted in this study examined the effects of relative humidity on molecular structure of the drug within the silica pores. In an effort to explore the hypothesis that water condensation was inducing a structural evolution of the drug, H-NMR scans of an imbibed tablet subjected to 100% relative humidity were taken. Specifically, fenofibrate was melted at 90.1°C on a glass plate atop a hot plate. A silica template made as previously described was placed on top of the melted drug, until the tablet was clear indicating complete imbibition. The imbibed tablet was removed from the melted drug, wiped off with a tissue, and placed in 0% relative humidity for three days. The tablet was then removed and cut into pieces small enough to fit in the sample tube. This was done with four sample tubes. Once loaded in the tubes, the tablets were moved to a glass chamber held at 100% relative humidity. After the H-NMR was calibrated and ready to generate T_2 and T_1T_2 plots, the appropriate sample tube was capped and placed in the magnet. Scans of the tablet were done after one, three, 7, and 14 days. T_2 plots from these samples are shown in Figure A.3.
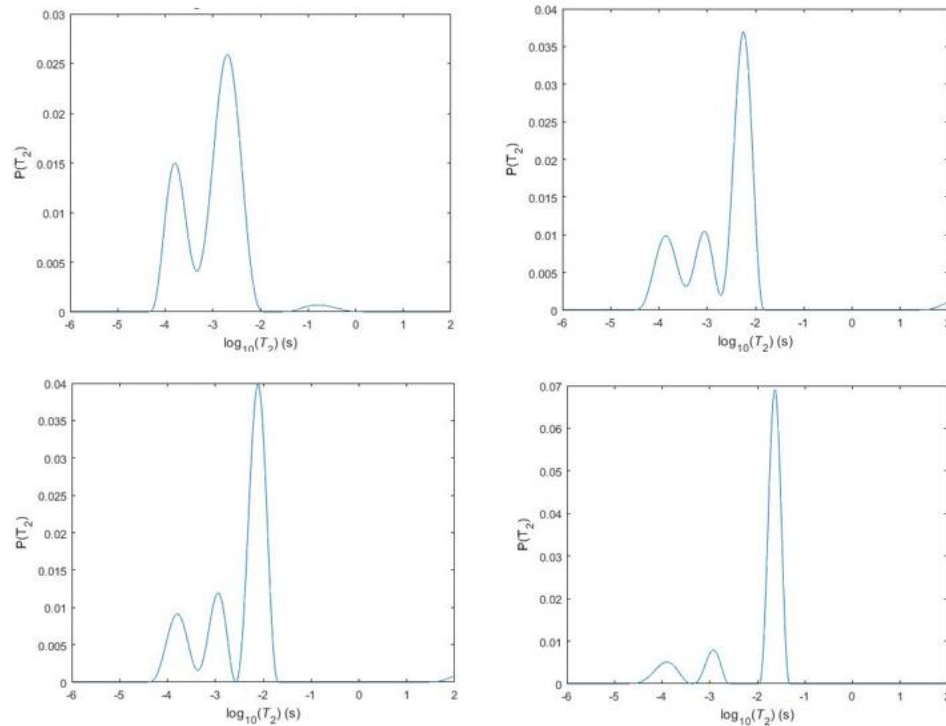
Figure A.3. H-NMR T_2 relaxation time scans of an imbibed tablet held at 100% relative humidity for one, three, seven and 14 days, showing the evolution of drug structure confined in pores. As time increases, water content increases and the two drug structures change conformation implying more restriction.

There are several obvious differences in the plots shown in Figure A.3. The first is the evolution of a third peak within the first three days. This implies three different populations within the pores of the silica. This may illustrate the condensation of water in the pores over time. The peak with the longest T_2 relaxation time was indicative of water, as that was the most mobile species in the tablets. The other two peaks are indicative of the drug structure. The peak with the shortest T_2 time indicated a more solid-like structure, possibly crystallized drug, while the longer T_2 time indicated a more liquid-like structure, possibly amorphous drug. When compared to the relaxation times of the previous figure showing the hypothesized evolution of amorphous drug to crystalline, the two left-most

peaks illustrate similar changes. It may also be true the shortest T_2 time indicated a pore containing a larger, more restricted crystal, while the longer T_2 time suggested a pore containing small, less restricted, crystals. If the latter was true, it would be supportive of the hypothesis of Oswald Ripening in the pores. The plots would indicate an evolution from smaller, less restricted crystals, to large, more restricted crystals, until an equilibrium was reached. It should also be noted that the analysis of the two smaller peaks becomes more difficult as the time scale is increased, due to the dwarfing effect of the increasing water peak intensity. To understand this evolution from amorphous to crystalline drug more clearly, T_1T_2 plots were generated as shown in Figure A.4.
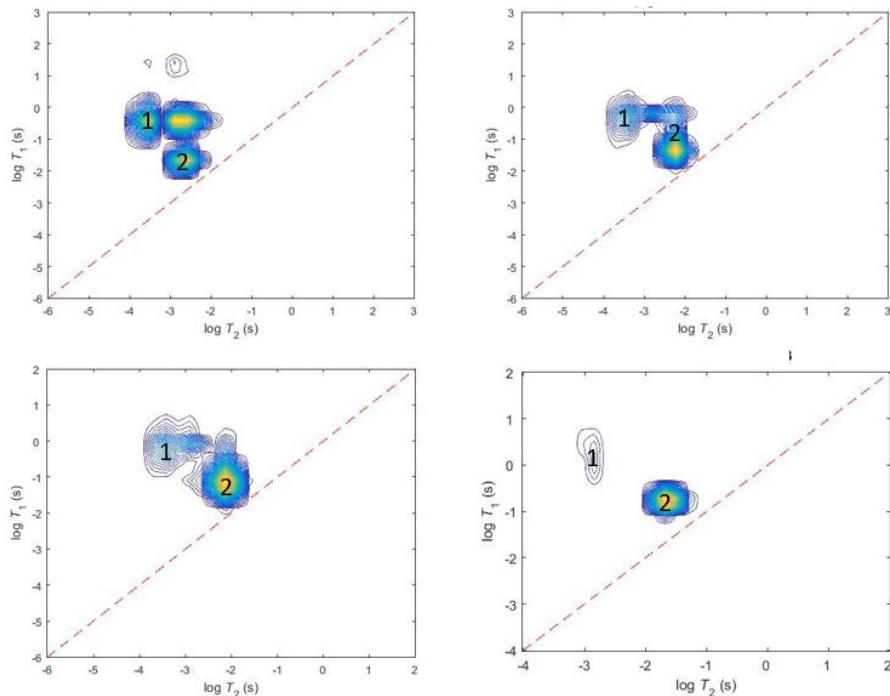

Figure A.4. T_1T_2 H-NMR scans of imbibed tablets kept at 100% relative humidity for (from left to right) one, three, 7, and 14 days. The changes in population distribution implies changes to the drug structure, with the water peak increasing in intensity as well as T_1 and T_2 times.

The first peak labeled above experiences decreased T_1 and T_2 times with respect to increased time in 100% relative humidity. These relaxation times indicate an evolution of a more solid-like substance. This agrees with the data in the previous figure, implying either amorphous drug is evolving into crystalline drug, or smaller crystals are becoming larger, more restricted crystals over time.

The second peak labeled in the plots above is representative of water within the pores. As time increases, the water peak increases in intensity as well as T_1 and T_2 relaxation times. This implies an increase in water content within the pores. This makes sense as the longer the imbibed tablet was in the 100% relative humidity chamber, the more water would be able to condense.

While H-NMR proves powerful as tool to analyze the local chemical and physical alterations, there has not been any conclusive evidence obtained from it. This method supports the idea of amorphous drug evolving into crystalline drug during quenching. Other data obtained from the H-NMR may imply a further evolution of amorphous drug with the induction of water condensation, or possibly an induced crystal size redistribution.

APPENDIX B

PRELIMINARY RAMAN SPECTROSCOPY DATA

Raman spectroscopy is a noninvasive tool that was used to understand the influence of relative humidity on the molecular structure and orientation of drug, fenofibrate, in composites. Changes in drug structure, induced by the controlled condensation of water, provide clues to the change in amorphous and crystalline content within the composite. This spectroscopy is conducted with a Ph.D. candidate in Dr. Rob Walker's laboratory group, Kyle Reeping, in the Chemistry and Biochemistry Department at Montana State University.

Raman Spectroscopy provides information about the composition and molecular structure of compounds.[18] It employs a laser and microscope to excite molecules within a substance, here the drug, silica tablet, and composite.[18] A laser is directed through a microscope objective onto the material, which subsequently interacts with the laser with respect to molecular energy modes such as vibrations.[19] The inelastically scattered light is filtered and analyzed, resulting in a spectrum of intensity versus Raman wavelength.[19] The "Raman wavelength," or "Raman shift," is dependent on the laser used, as different vibrational modes are captured with different lasers.[19] Due to this, only spectra obtained using the same laser and excitation times are comparable. Additionally, each unique peak corresponds to a different molecular arrangement, and thus different vibrational properties due to bond arrangements.[18] This allows spectral peaks to be compared to known peak wavenumbers to identify the composition and structure. Unfortunately, if a spectral peak has not been conclusively identified, it is unlikely that it can be used to identify the composition and/or arrangement or a complex system conclusively. Due to the complicated nature of the spectra obtained, as well as the unknown identifiable peaks, in the following

experiments, only comparative analysis is conducted. While there is minimal literature about the exact identification of peaks in the spectrum, a paper published in 2009 suggested analysis of structural changes of the drug.[20] Spectral peak widening of the composite in a varied relative humidity suggests a decrease in crystalline drug content.[20] Additionally, if the wavenumber associated with the peak changes, it implies a change in the crystalline or amorphous form.[20]

The difference between an unimbibed and imbibed tablet was examined using Raman spectroscopy as a baseline for future experiments. It is important to understand what changes in the spectrum are due to the drug, and what are due to the silica. To explore this, a silica tablet was slip cast and left in 0.0 relative humidity for three days. Another silica tablet was slip cast and imbibed with fenofibrate at 90°C. This composite was then wiped off with a tissue and placed in 0.0 relative humidity for three days. In all experiments, unless otherwise noted, a 633 nm laser was used and all samples were placed on top of a gold disc to restrict unwanted light refraction. Scans of the samples were taken every 15 seconds, in multiples of three before moving to the next sample. This was done to eliminate cosmic rays. If an abrupt signal appeared with a width less than one wavelength, that then disappeared after the next scan, it was labeled a cosmic ray and removed. The two spectra are displayed in Figure B.1., showing the complex nature of the composite as compared to the silica template. This plot allowed us to subtract out the signal from the silica, since we are only interested in the changes the fenofibrate is undergoing.
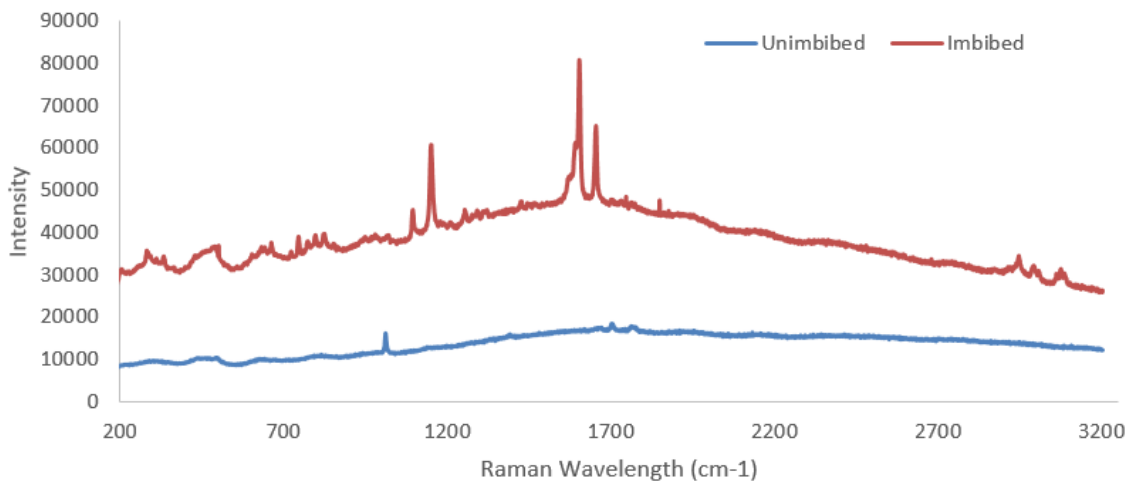
Figure B.1. Raman spectra of an unimbibed silica tablet and fenofibrate imbibed silica tablet, illustrating the difference in drug imbibition and complex nature of the system.

The next spectrum needed was the difference between restricted and unrestricted fenofibrate. This was important to understand what spectral changes were due to the drug undergoing melting and recrystallization, and what were due to drug confinement in nanopores. To understand this, a slip cast silica tablet was imbibed as previously described, and placed in 0.0 relative humidity for three days. Additionally, fenofibrate was melted on a glass slide at 90°C, and the slide was subsequently moved to 0.0 relative humidity for three days. Raman spectra were then obtained for these two samples, as previously described. These spectra are displayed together, illustrating the effect confinement has on the drug in the system. There is a noticeably lower intensity in the Raman spectrum associated with the restricted drug. This depletion dilutes the effects of peak widening and narrowing, making conclusions difficult to draw.
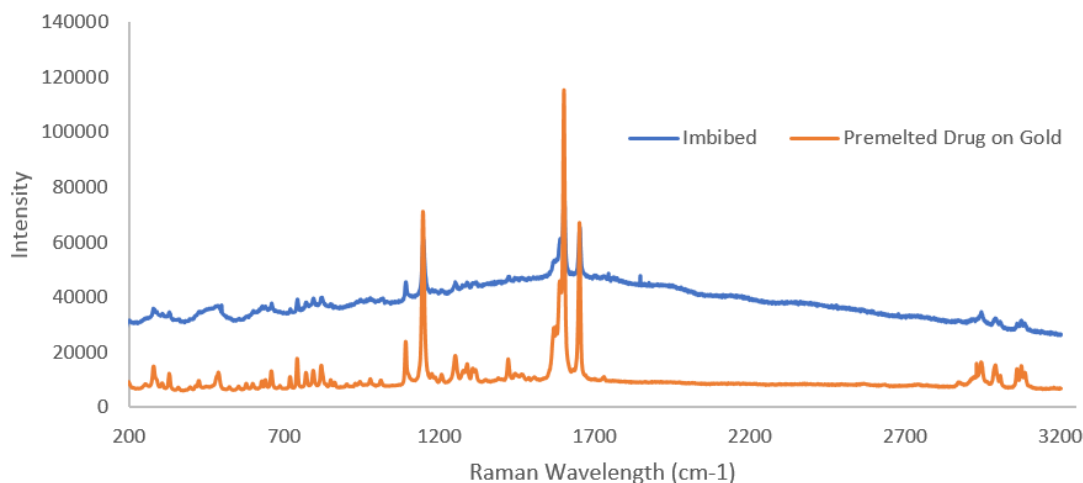
Figure B.2. Raman spectra (633 nm) of a fenofibrate imbibed silica tablet coplotted with unconfined fenofibrate that underwent the same protocol, showing the intensity depletion of confined fenofibrate.

While differential scanning calorimetry (DSC) proves useful, it is unable to provide insight into the molecular changes occurring when a tablet is subjected to 0.0 relative humidity and then varying relative humidity, without returning to 0.0 relative humidity. To investigate the effect this change in protocol had on the molecular structure, Raman spectroscopy was conducted on six different tablets as previously described. The difference in this protocol is that the tablets never returned to 0.0 relative humidity. In other words, they were imbibed, placed in 0.0 relative humidity for three days, then varying relative humidities for three days. They were then tested. In order to ensure no water evaporates off due to the humidity change between the chamber they were stored in and the testing chamber, the corresponding saturated salt solution was placed in the testing chamber for ten minutes to allow for equilibration. This was done in the order of lowest relative humidity to highest.

To support the hypothesis that crystallinity isn't changing drastically in samples exposed to differing relative humidities, and to try to understand possible other molecular changes occurring, Raman spectroscopy was performed on six different tablets. The silica tablets were made as previously described – slip cast on gypsum. The porous silica tablets were then placed on melted fenofibrate, melted at 90ºC, until fully imbibed, about 30 minutes. The imbibed tablets were then removed with tweezers and quickly wiped off with tissue. They were then placed in a 0.0 relative humidity chamber for three days. After this, they were transferred to varying relative humidity chambers for three days. The following relative humidities were used: 0.0, 0.25, 0.43, 0.75, 0.91, and 1.0. All composites were finally moved back to the 0.0 relative humidity chamber for three days. Following this, they were transferred to the Raman spectroscopy facility.

If the hypothesis that crystallinity is undergoing no drastic change, the peak widths and Raman wavelength corresponding to the maximum intensity won't change. This is what happened, as shown in Figure B.3. The peaks are all similar in width and Raman wavelength, indicating no significant change in crystallinity was induced by varying the relative humidity.
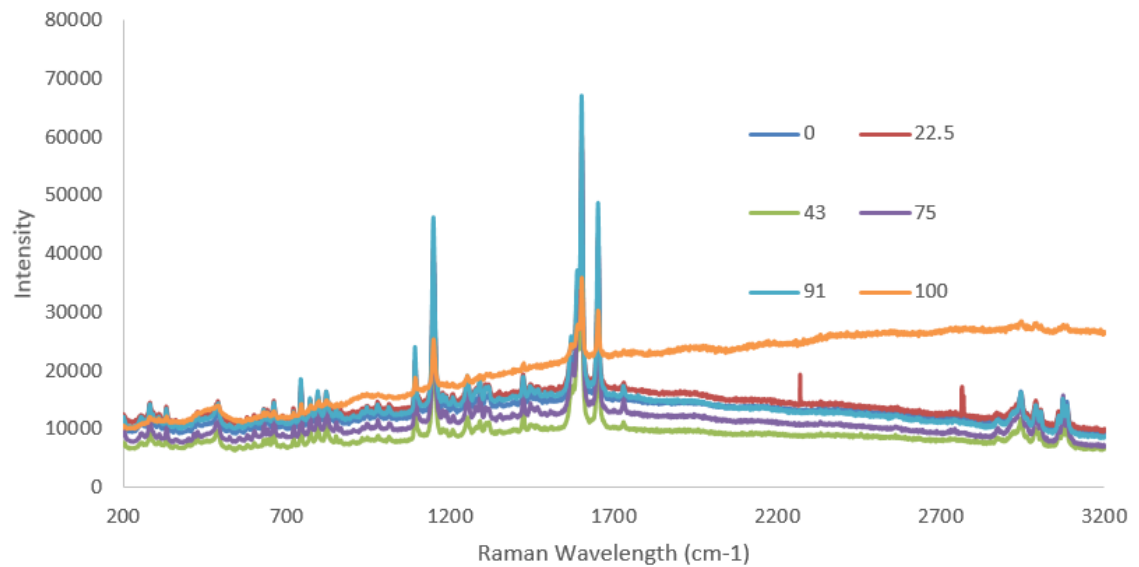
Figure B.3. Raman spectrum (633 nm) of composites that underwent the protocol of imbibition, 0.0 relative humidity, varying relative humidity, then 0.0 relative humidity. These spectra show minimal differences in molecular composition and arrangement.

As previously elaborated, crystallinity changes would be indicated by changing peak width, and Raman wavelength number. Figure B.4 displays the spectra produced by these composites, and show no discernable changes with respect to varying relative humidities. This implies no drastic structural changes were induced by differing humidities.
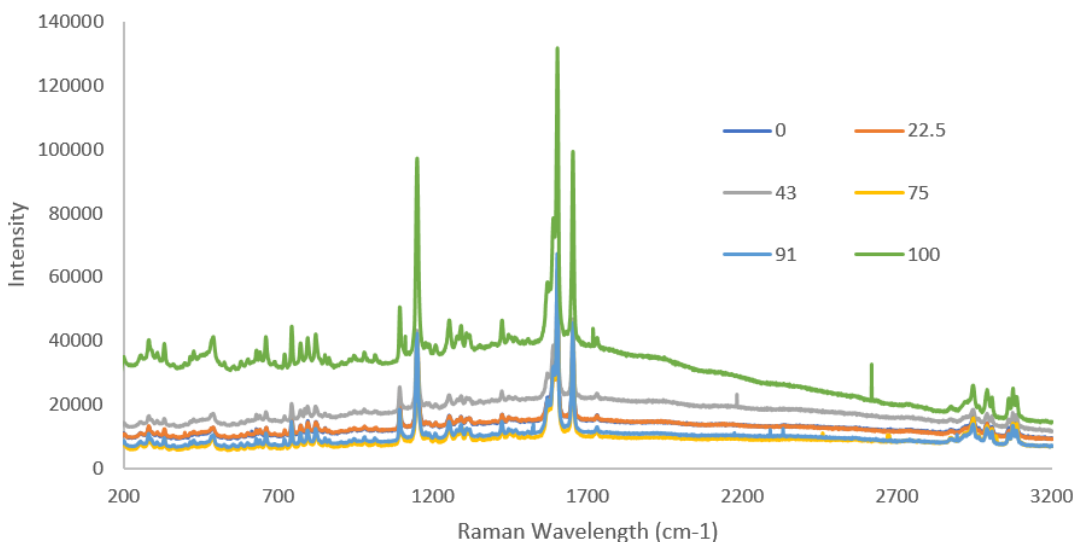
Figure B.4. Raman spectra (633 nm) of fenofibrate imbibed silica tablets coplotted that are subjected to varying relative humidities. These composites are subjected to 0.0 relative humidity then varying relative humidities before testing. This shows no meaningful change in molecular arrangement with respect to relative humidity.

While there were few notable differences in spectra of varying relative humidity within the same protocol, there were major differences between spectra of varying relative humidity with respect to protocol. As shown subsequently in Figure B.5, the spectra of a tablet at 1.0 relative humidity was examined across protocols. There is a dramatic depletion of intensity in the peaks seen in the spectra that went from 0.0 to 1.0 back to 0.0 relative humidity as compared to staying in 1.0 relative humidity. While it may appear as though signals disappear, this is not the case. The spectrum of these signals is dwarfed by the dominating spectrum of the protocol ending in 1.0 relative humidity. The signal in this spectrum occurring at about 2650 cm^{-1} is a cosmic ray, identified due to its near-zero width. The obvious diminished peak intensity and width in the protocol ending in 0.0 relative humidity, implies the composite ending in 1.0 humidity is composed of less crystalline structure. However, due to the inequality of peak intensity, it is difficult to compare exact

peak widths. The differences in spectra are from molecular changes of confined fenofibrate, so while there are no conclusions drawn it is clear the drug undergoes changes with the induction of water. It is also possible that structural changes are happening so slowly that an additional three days between imbibition and testing, in the protocol of 0.0, 1.0, 0.0 relative humidity, allowing for more conformational changes.
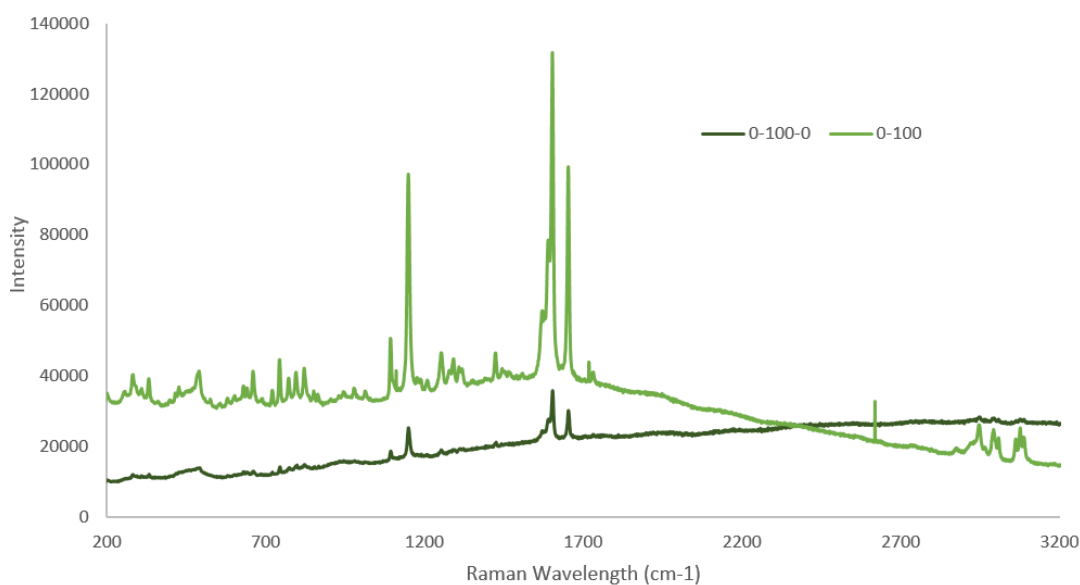

Figure B.5. Raman spectra (633 nm) of fenofibrate imbibed silica tablets that underwent differing protocols. This shows the depletion in intensity, implying an alteration in molecular drug arrangement in the composite that was exposed to 0.0 relative humidity, 1.0 relative humidity, and 0.0 relative humidity again.

System analysis using Raman spectroscopy proved useful in conveying molecular changes in fenofibrate restricted by pores, provided by colloidal silica, compared to unconfined drug. Raman spectroscopy also proved useful in gaining insight to the molecular changes induced by varying relative humidity composites were exposed to. Two different protocols were investigated. The first was exposing the composites to 0.0 relative humidity, then varying relative humidity, and finally 0.0 relative humidity again, all for

equal time. The second was exposing the composites to 0.0 relative humidity and then varying relative humidity, foregoing re-exposure to 0.0, both for equal time. While there are, seemingly, no drastic changes with respect to differing relative humidities within each protocol, there are definite changes in spectra with respect to protocols. Exposing a composite to non-zero relative humidity increases the peak intensity greatly.

REFERENCES CITED

1   Desarnaud, J., Bonn, D. & Shahidzadeh, N. The Pressure induced by salt crystallization in confinement. *Scientific Reports* **6**, 30856, doi:10.1038/srep30856

https://www.nature.com/articles/srep30856#supplementary-information (2016).

2   Roger, E., Lagarce, F. & Benoit, J.-P. Development and characterization of a novel lipid nanocapsule formulation of Sn38 for oral administration. *Eur J Pharm Biopharm* **79**, 181-188, doi:10.1016/j.ejpb.2011.01.021 (2011).

3   Amidon, G. L., Lennernäs, H., Shah, V. P. & Crison, J. R. A Theoretical Basis for a Biopharmaceutic Drug Classification: The Correlation of in Vitro Drug Product Dissolution and in Vivo Bioavailability. *Pharmaceutical Research* **12**, 413-420, doi:10.1023/a:1016212804288 (1995).

4   Fagerholm, U. The Role of Permeability in Drug ADME/PK, Interactions and Toxicity—Presentation of a Permeability-Based Classification System (PCS) for Prediction of ADME/PK in Humans. *Pharmaceutical Research* **25**, 625-638, doi:10.1007/s11095-007-9397-y (2008).

5   Pouton, C. W. Lipid formulations for oral administration of drugs: non-emulsifying, self-emulsifying and 'self-microemulsifying' drug delivery systems. *European Journal of Pharmaceutical Sciences* **11, Supplement 2**, S93-S98, doi:http://doi.org/10.1016/S0928-0987(00)00167-6 (2000).

6   Gupta, S., Kesarla, R. & Omri, A. Formulation Strategies to Improve the Bioavailability of Poorly Absorbed Drugs with Special Emphasis on Self-Emulsifying Systems. *ISRN Pharmaceutics* **2013**, 16, doi:10.1155/2013/848043 (2013).

7   Savjani, K. T., Gajjar, A. K. & Savjani, J. K. Drug Solubility: Importance and Enhancement Techniques. *ISRN Pharmaceutics* **2012**, 195727, doi:10.5402/2012/195727 (2012).

8   Serajuddin, A. T. M. Salt formation to improve drug solubility. *Advanced Drug Delivery Reviews* **59**, 603-616, doi:http://dx.doi.org/10.1016/j.addr.2007.05.010 (2007).

9   Chaumeil, J. C. Micronization: a method of improving the bioavailability of poorly soluble drugs. *Methods and findings in experimental and clinical pharmacology* **20**, 211-215 (1998).

10   Style, R. W., Peppin, S. S. L., Cocks, A. C. F. & Wettlaufer, J. S. Ice-lens formation and geometrical supercooling in soils and other colloidal materials. *Physical Review E* **84**, 041402 (2011).

11   Giulietti, M., Seckler, M. M., Derenzo, S., Ré, M. I. & Cekinski, E. INDUSTRIAL CRYSTALLIZATION AND PRECIPITATION FROM SOLUTIONS: STATE OF THE TECHNIQUE. *Brazilian Journal of Chemical Engineering* **18**, 423-440 (2001).

12   Greenspan, L. Humidity Fixed-Points of Binary Saturated Aqueous-Solutions. *J Res Nbs a Phys Ch* **81**, 89-96, doi:10.6028/jres.081A.011 (1977).

13   Clas, S.-D., Dalton, C. R. & Hancock, B. C. Differential scanning calorimetry: applications in drug development. *Pharmaceutical Science & Technology Today* **2**, 311-320, doi:http://doi.org/10.1016/S1461-5347(99)00181-9 (1999).

14   Górniak, A., Wojakowska, A., Karolewicz, B. & Pluta, J. Phase diagram and dissolution studies of the fenofibrate–acetylsalicylic acid system. *Journal of Thermal Analysis and Calorimetry* **104**, 1195-1200, doi:10.1007/s10973-010-1148-3 (2011).

15   Vetter, T., Iggland, M., Ochsenbein, D. R., Hänseler, F. S. & Mazzotti, M. Modeling Nucleation, Growth, and Ostwald Ripening in Crystallization Processes: A Comparison between Population Balance and Kinetic Rate Equation. *Crystal Growth & Design* **13**, 4890-4905, doi:10.1021/cg4010714 (2013).

16   Steiger, M. Crystal growth in porous materials—II: Influence of crystal size on the crystallization pressure. *Journal of Crystal Growth* **282**, 470-481, doi:http://doi.org/10.1016/j.jcrysgro.2005.05.008 (2005).

17   Bloembergen, N. & Morgan, L. O. Proton Relaxation Times in Paramagnetic Solutions. Effects of Electron Spin Relaxation. *The Journal of Chemical Physics* **34**, 842-850, doi:10.1063/1.1731684 (1961).

18   Downes, A. & Elfick, A. Raman Spectroscopy and Related Techniques in Biomedicine. *Sensors* **10**, 1871 (2010).

19   Ramos, I., #xea, Martins, s. R., Malkin, A. & Lyng, F. M. Current Advances in the Application of Raman Spectroscopy for Molecular Diagnosis of Cervical Cancer. *BioMed Research International* **2015**, 9, doi:10.1155/2015/561242 (2015).

20   Heinz, A., Gordon, K. C., McGoverin, C. M., Rades, T. & Strachan, C. J. Understanding the solid-state forms of fenofibrate – A spectroscopic and computational study. *European Journal of Pharmaceutics and Biopharmaceutics* **71**, 100-108, doi:http://dx.doi.org/10.1016/j.ejpb.2008.05.030 (2009).